Wind properties of Milky Way and SMC massive stars: empirical Z dependence from cmfgen models

W.L.F. Marcolino, J.-C. Bouret, H.J. Rocha-Pinto, M. Bernini-Peron, J.S. Vink

Monthly Notices of the ROYAL ASTRONOMICAL SOCIETY

MNRAS **511,** 5104–5119 (2022) https://doi.org/10.1093/mnras/stac452
Advance Access publication 2022 February 18

Wind properties of Milky Way and SMC massive stars: empirical Z dependence from CMFGEN models

W. L. F. Marcolino,[1]★ J. -C. Bouret,[2] H. J. Rocha-Pinto,[1] M. Bernini-Peron[1,3] and J. S. Vink[4]

[1]*Observatório do Valongo, Universidade Federal do Rio de Janeiro, Ladeira Pedro Antônio, 43, CEP 20080-090, Rio de Janeiro, Brazil*
[2]*Aix-Marseille Université, CNRS, CNES, LAM, F-13007 Marseille, France*
[3]*Zentrum für Astronomie der Universität Heidelberg, Astronomisches Rechen-Institut, Mönchhofstr. 12-14, D-69120 Heidelberg, Germany*
[4]*Armagh Observatory and Planetarium, College Hill, Armagh BT61 9DG, Northern Ireland*

Accepted 2022 February 13. Received 2022 January 28; in original form 2021 October 15

ABSTRACT

Detailed knowledge about stellar winds and evolution at different metallicities is crucial for understanding stellar populations and feedback in the Local Group of galaxies and beyond. Despite efforts in the literature, we still lack a comprehensive, empirical view of the dependence of wind properties on metallicity (Z). Here, we investigate the winds of O and B stars in the Milky Way (MW) and Small Magellanic Cloud (SMC). We gathered a sample of 96 stars analysed by means of the NLTE code CMFGEN. We explored their wind strengths and terminal velocities to address the Z dependence, over a large luminosity range. The empirical wind–luminosity relation (WLR) obtained updates and extends previous results in the literature. It reveals a luminosity and Z dependence, in agreement with the radiatively driven wind theory. For bright objects ($\log L/L_{\odot} \gtrsim 5.4$), we infer that $\dot{M} \sim Z^{0.5-0.8}$. However, this dependence seems to get weaker or vanish at lower luminosities. The analysis of the terminal velocities suggests a shallow Z^n dependence, with $n \sim 0.1-0.2$, but it should be confirmed with a larger sample and more accurate V_{∞} determinations. Recent results on SMC stars based on the PoWR code support our inferred WLR. On the other hand, recent bow-shocks measurements stand mostly above our derived WLR. Theoretical calculations of the WLR are not precise, specially at low L, where the results scatter. Deviations between our results and recent predictions are identified to be due to the weak wind problem and the extreme terminal velocities predicted by the models. The Z dependence suggested by our analysis deserves further investigations, given its astrophysical implications.

Key words: stars: atmospheres – stars: fundamental parameters – stars: massive – stars: mass-loss – stars: winds, outflows.

1 INTRODUCTION

The winds of massive stars are mostly driven by the transference of momentum from their intense UV radiation field to metal lines (Castor, Abbott & Klein 1975; Lamers & Cassinelli 1999). A late-type O star at solar metallicity, for example, has its wind driven mainly by Fe (∼23 per cent), Si (∼20 per cent), C (∼14 per cent), Al (∼13 per cent), and other metal (few per cent) lines. H and He correspond only to ∼13 and ∼0.05 per cent of the radiative force, respectively (Mokiem et al. 2007). Due to this fact, massive stars in lower metallicity environments are expected – and in fact observed – to have weaker winds (Vink, de Koter & Lamers 2001; Mokiem et al. 2007). These winds represent a significant amount of mass lost even during the relatively short lifetime of massive stars (Ekström et al. 2012). Moreover, they have an enormous impact in the ISM through mechanical energy and chemical elements deposition (Abbott 1982).

In addition to their metallicity (Z) dependence, stellar winds are coupled with rotation. The mass-loss rate can be affected by rotation and at the same time, remove angular momentum, changing the internal rotation profile (Meynet & Maeder 2000). In contrast with low-mass stars ($M \lesssim 8\,M_{\odot}$), single massive star evolution is thus a complex function of the initial mass, Z, mass-loss, and rotation. Such dependence is challenging to describe and implement in models, but several efforts have been made in the literature (e.g. Brott et al. 2011; Ekström et al. 2012; Georgy et al. 2013). In fact, if we aim to understand topics such as stellar populations and feedback at low and high redshifts, production of local pair instability supernovae (e.g. Whalen et al. 2014), or even the origin of the masses of the binary components that produce gravitational waves detected by LIGO (see e.g. Abbott et al. 2016), we must have also a quantitative understanding of stellar evolution and winds at different metallicities.

From an observational point of view, Mokiem et al. (2007) were the first to present a detailed comparison of wind strengths of massive OB stars at different metallicities. In particular, they analysed several data from the Milky Way (MW), Large Magellanic Cloud (LMC), and Small Magellanic Cloud (SMC). A clear mass-loss rate dependence on Z was observed and the following relation was inferred: $\dot{M} \propto Z^{0.83\pm0.16}$, in agreement with the theoretical predictions of Vink et al. (2001) within the error bars, namely, $\dot{M} \propto Z^{0.69\pm0.10}$. This agreement provided a solid framework for the use of the theoretical mass-loss recipes in stellar evolution models. However, recent works by Björklund et al. (2021) and Vink & Sander (2021), for example, provide different dependences, $\dot{M} \propto Z^{0.95}$ and $\dot{M} \propto Z^{0.42}$, respectively, revealing mismatch among theoretical calculations. To date, the work of Mokiem et al. (2007)

★ E-mail: wagner@astro.ufrj.br

is still the most comprehensive one on the empirical metallicity dependence of the winds of massive OB stars.

Newer high-resolution, multiwavelength data of hundreds of galactic and extragalactic O and B stars were analysed during the last decade. Different codes and methods were applied to infer the stellar and wind parameters of these objects, addressing important questions for stellar evolution and wind theory. Fast, robust, stellar atmosphere analyses of large observational data sets were performed (e.g. Sabín-Sanjulián et al. 2017; Ramírez-Agudelo et al. 2017), but often at the expense of wavelength coverage (e.g. only optical). In parallel, detailed, computational demanding analyses of multiwavelength data of much smaller samples were carried out with co-moving frame, full metal line-blanketing calculations (e.g. Bouret et al. 2013; Marcolino et al. 2017; Bouret et al. 2021). Despite all these efforts in the MW and in the Magellanic Clouds, we still lack a complete, updated view of the empirical dependence of wind properties on Z. Part of the problem is related to the lack of quantitative UV analyses of low-luminosity O and B stars, not taken into account in Mokiem et al. (2007) and other studies, as we will further discuss.

Our aim in this paper is to provide an updated, improved view of the metallicity dependence of the winds of O and B stars. To do so, we gathered the results of the analysis of 96 O and B stars, either in the MW or in the SMC, all performed with the code CMFGEN (Hillier & Miller 1998). This allows us to achieve a robust internal consistency, in the sense that the physical properties of the stars were measured with the same code, under the same basic physical ingredients and assumptions (see below).

We explore wind–luminosity relation (WLR) diagrams and discuss the results in terms of the MW and SMC metallicity. We analyse the Z dependence in detail over a large luminosity range. We also analyse the terminal velocity (V_∞) of the stars of our sample. We estimated the m and n exponents in the $V_\infty \propto Z^n$ and $\dot{M} \propto Z^m$ relations, which are widely used in the literature. We also compare our results with other techniques and measurements for O and B stars in the MW and SMC.

In Section 2, we describe our sample and present our WLR analysis for the MW and SMC stars. The metallicity dependence of the mass-loss rate is presented later in Section 3. In Section 4, the terminal velocities in the MW and SMC are presented along with a $V_\infty(Z)$ analysis. In Section 5, we discuss our results, possible caveats, and other measurements in the literature (e.g. data of SMC stars obtained with the PoWR code and bow-shocks measurements of MW stars). We also compare our empirical data with theoretical results to check for trends and highlight possible problems. Finally, in Section 6, we present a summary of our main findings.

2 STELLAR WIND STRENGTHS – MILKY WAY AND SMC

2.1 Observational data

In this paper, we focus on a comparison of the wind properties of O and B stars in the MW and SMC, these populations offer the wider span in metallicity.

We selected several studies of O and B stars in both galaxies from the literature (Crowther et al. 2006; Searle et al. 2008; Marcolino et al. 2009, 2017; Bouret et al. 2012, 2013, 2021; Martins et al. 2012, 2015; Mahy et al. 2015; de Almeida et al. 2019), all relying on detailed joint analysis of UV and optical spectra performed with CMFGEN (Hillier & Miller 1998). Most of them were done by our group during the last decade.

We present our sample in Tables 1 and 2. In total, we gathered 60 MW stars and 36 SMC stars. Early- to late-type O stars of all main luminosity classes are comprised (I, III, and V). Most B stars are supergiants, with the exception of two sub-giants and one giant in the SMC. Details regarding the physical parameters present in these tables will be discussed in the next section.

For visualization purposes, we present in Fig. 1 the location of these stars in the Hertzsprung–Russell (H-R) diagram. We also include evolutionary tracks with rotation for $Z = 0.014$ (solar metallicity) from Ekström et al. (2012) and $Z = 0.002$ (appropriate for SMC) from Georgy et al. (2013). These tracks follow from models with the same physical ingredients, e.g. $V_{\rm ini}/V_{\rm crit} = 0.4$, convection parameters, and nuclear reaction rates (for more details, see Georgy et al. 2013). A large interval in effective temperature and luminosity is covered and there is a fair number of stars in each of the luminosity classes (I, III, and V). Moreover, as expected, the different classes occupy different loci in the H-R diagram.

By selecting studies performed with the same atmospheric code, which are based on the same basic set of physical assumptions, we ensure that the results we analyse have internal consistency. On the other hand, we acknowledge that systematics and biases related to the details of the spectroscopic analysis methodology and what data were available for the analysis, are impossible to grasp at this point.

For example, the CMFGEN models used present a certain degree of diversity. Some works do not adopt the same atomic data (i.e they use different ion models with various number of transitions, energy levels, and superlevels), or they do not consider the same set of chemical elements, or use a different version of the code (this last point should not be an issue). In addition, although the effective set of sensitive spectral lines useful to characterize the photospheric and wind properties of O and B stars is common knowledge (see e.g. Martins 2011), the selected studies used less or more diagnostics than others for a specific parameter, depending on the availability and/or quality of the data. Ideally, a tailored re-analysis of the whole sample should be done with fully homogeneous modelling assumptions and new observational data, but this beyond the scope of the paper.

For galactic stars, most works (see refs above) relied on UV data from the *IUE* and FUSE satellites. *IUE* observations are mainly from the short-wavelength spectrograph (SWP) (∼1150–2000 Å), with resolving power $R \sim 10\,000$. FUSE spectra are mainly from the LiF2A channel (∼1086–1183 Å), with $R \sim 20\,000$. This channel contains the PV λλ1118, 1128 doublet, whose behaviour lead Fullerton, Massa & Prinja (2006) to uncover the P v problem, i.e the discordance between mass-loss rates derived from P v with those obtained from Hα, which subsequently triggered an extensive research on wind clumping as a solution of this problem (see Puls, Vink & Najarro 2008, for a review). Note that Copernicus data were also used for a few Galactic stars (e.g. Marcolino et al. 2009; Bouret et al. 2012), when FUSE data were not available.

For SMC stars, the *HST* observations were acquired with COS (Cosmic Origins Spectrograph, $R \sim 20\,000$) or STIS (Space Telescope Imaging Spectrograph, $R \sim 40\,000$). FUSE data are also available for some stars.

Most optical observations are also of high-resolution (with resolving power $R \gtrsim 40\,000$) but intermediate-resolution (resolving power $R \sim 6000$–$10\,000$) was also used (mostly for B supergiants; see Crowther et al. 2006; Searle et al. 2008). There are only a few exceptions where either the optical spectrum is missing or it is obtained at relatively low spectral resolving power ($R \sim 2000$; 2dF spectra) (e.g. in Bouret et al. 2013, 2021). Note that for some stars, the mid-IR were also modelled (Marcolino et al. 2017). This multiwavelength aspect is fundamental to measure values of physical parameters of interest with the highest fidelity.

Table 1. Stellar and wind parameters of MW O and B stars analysed with CMFGEN models.

Star	SpT	$\log L/L_\odot$	$T_{\rm eff}$ (kK)	$R/R_\odot$	$\log \dot{M}$ ($\log \dot{M}_{\rm H\alpha}$)	V_∞ (km s^{-1})	$\log D$ ($\log D_{\rm H\alpha}$)	Reference
HD 16691	O4If	5.94 ± 0.1	41.0	18.66	−4.91	2300	29.89 ± 0.06	B12
HD 66811	O4I	5.91 ± 0.1	40.0	18.94	−5.05	2300	29.75 ± 0.06	B12
HD 190429A	O4If	5.96 ± 0.1	39.0	21.10	−4.98	2300	29.84 ± 0.05	B12
HD 15570	O4If	5.94 ± 0.1	38.0	21.72	−5.01	2200	29.80 ± 0.05	B12
HD 14947	O4.5If	5.83 ± 0.1	37.0	20.19	−5.09	2300	29.72 ± 0.07	B12
HD 210839	O6I	5.80 ± 0.1	36.0	20.60	−5.20	2100	29.58 ± 0.09	B12
HD 163758	O6.5If	5.76 ± 0.1	34.5	21.42	−5.15	2100	29.64 ± 0.08	B12
HD 192639	O7.5Iabf	5.68 ± 0.1	33.5	20.72	−5.27	1900	29.47 ± 0.10	B12
HD 188001	O7.5Iaf	5.69 ± 0.20	33.0	21.60	−5.23	1800	29.49 ± 0.41	M17
HD 207198	O8.5II	5.05 ± 0.26	32.5	10.66	−7.00	2000	27.61 ± 0.41	M17
HD 30614	O9.5Iab	5.81 ± 0.25	29.0	32.34	−5.12	1600	29.64 ± 0.41	M17
HD 188209	O9.5Iab	5.65 ± 0.26	30.0	25.30	−5.75	2000	29.05 ± 0.41	M17
HD 209975	O9.5Ib	5.35 ± 0.30	30.5	17.10	−6.50	2000	28.22 ± 0.41	M17
HD 195592	O9.7Ia	5.47 ± 0.25	28.0	23.29	−5.14	1400	29.49 ± 0.41	M17
HD 91969	B0Ia	5.52 ± 0.25	27.5	25.3	(−6.00)	1470	(28.67 ± 0.15)	C06
HD 94909	B0Ia	5.49 ± 0.25	27.0	25.5	(−5.70)	1050	(28.62 ± 0.15)	C06
HD 122879	B0Ia	5.52 ± 0.25	28.0	24.4	(−5.52)	1620	(29.18 ± 0.15)	C06
HD 38771	B0.5Ia	5.35 ± 0.25	26.5	22.2	(−6.05)	1525	(28.61 ± 0.15)	C06
HD 115842	B0.5Ia	5.65 ± 0.25	25.5	34.2	(−5.70)	1180	(28.94 ± 0.15)	C06
HD 152234	B0.5Ia	5.87 ± 0.25	26.0	42.4	(−5.57)	1450	(29.21 ± 0.15)	C06
HD 192660	B0Ib	5.74 ± 0.13	30.0	23.4	(−5.30)	1850	$(29.45^{+0.00}_{-0.40})$	S08
HD 204172	B0.2Ia	5.48 ± 0.27	28.5	22.4	(−6.24)	1685	$(28.46^{+0.34}_{-0.40})$	S08
HD 185859	B0.5Ia	5.54 ± 0.14	26.0	29.1	(−6.30)	1830	$(28.49^{+0.08}_{-0.10})$	S08
HD 213087	B0.5Ib	5.69 ± 0.11	27.0	32.0	(−6.15)	1520	$(28.58^{+0.20}_{-0.00})$	S08
HD 64760	B0.5Ib	5.48 ± 0.26	28.0	23.3	(−5.96)	1600	$(28.73^{+0.27}_{-1.04})$	S08
ϵ Ori	B0Iab	5.60 ± 0.33	27.5	28.0	−5.60	1800	29.18 ± 0.22	M15a
HD 167264	B0.5Iab	5.65 ± 0.27	28.0	28.6	−6.00	2000	28.83 ± 0.21	M15a
HD 156292	O9.7III	5.12 ± 0.20	31.0	13.0	−8.32	1300	$26.15^{+0.56}_{-0.48}$	A19
HD 24431	O9III	5.17 ± 0.20	33.0	11.9	−8.10 (−6.27)	2300	26.60 $(28.12^{+0.49}_{-0.49})$	A19
HD 105627	O9III	5.17 ± 0.20	33.0	11.9	−7.89	2100	$26.74^{+0.72}_{-0.40}$	A19
HD 116852	O8.5II-III((f))	5.33 ± 0.20	32.5	14.7	−6.72	2100	$27.98^{+0.62}_{-0.60}$	A19
HD 153426	O8.5III	5.24 ± 0.20	32.0	13.7	−7.85 (−6.35)	2400	26.90 $(28.39^{+0.52}_{-0.35})$	A19
HD 218195	O8.5IIINstr	5.24 ± 0.20	33.0	12.9	−7.49 (−6.39)	2000	27.16 $(28.27^{+0.52}_{-0.61})$	A19
HD 36861	O8III	5.30 ± 0.20	33.5	13.4	−7.10 (−6.39)	2000	27.56 $(28.28^{+0.38}_{-0.92})$	A19
HD 115455	O8III((f))	5.30 ± 0.20	34.0	13.0	−7.80 (−6.15)	2300	26.92 $(28.36^{0.49}_{0.49})$	A19
HD 135591	O8IV((f))	5.10 ± 0.20	35.0	9.7	−7.20	2100	$27.41^{+0.60}_{-1.12}$	A19
HD 193514	O7-7.5III	5.65 ± 0.09	34.5	18.7	−5.60	2190	29.18 ± 0.48	M15b
HD 193682	O5III(f)	5.50 ± 0.09	39.4	12.1	−5.70	2650	29.06 ± 0.48	M15b
HD 190864	O6.5III(f)	5.35 ± 0.14	38.0	10.9	−6.40	2250	28.27 ± 0.48	M15b
HD 191978	O8III	5.35 ± 0.23	33.2	14.3	−8.70	1600	25.88 ± 0.48	M15b
HD 216898	O9IV-O8.5V	4.72 ± 0.25	34.0	6.7	−9.35	1700	25.09 ± 0.71	M09
HD 326329	O9V	4.74 ± 0.10	31.0	8.0	−9.22	1700	25.26 ± 0.71	M09
HD 66788	O8-9V	4.96 ± 0.25	34.0	8.7	−8.92	2200	25.69 ± 0.71	M09
ζ Oph	O9.5Vnn	4.86 ± 0.10	32.0	9.2	−8.80	1500	25.66 ± 0.71	M09
HD 216532	O8.5V((n))	4.79 ± 0.25	33.0	7.5	−9.22	1500	25.19 ± 0.72	M09
HD 46223	O4V((f))	5.60 ± 0.11	43.0	11.47	−6.67 (−5.70)	2800	28.11 (29.08 ± 0.48)	M12
HD 46150	O5V((f))z	5.65 ± 0.25	42.0	12.73	−6.80 (−5.90)	2800	28.00 (28.90 ± 0.48)	M12
HD 46485	O7Vn	5.05 ± 0.11	36.0	8.69	−7.80 (−6.45)	1850	26.74 (28.09 ± 0.48)	M12
HD 46202	O9.5V	4.85 ± 0.12	33.5	7.97	−9.00 (−7.10)	1200	25.33 (27.23 ± 0.48)	M12
HD 48279	ON8.5V	4.95 ± 0.11	34.5	8.43	−8.80 (−6.80)	1300	25.58 (27.58 ± 0.48)	M12
HD 46966	O8.5IV	5.20 ± 0.11	35.0	10.92	−8.00 (−6.40)	2300	26.68 (28.28 ± 0.48)	M12
HD 38666	O9.5V	$4.66^{+0.40}_{-0.30}$	33.0	6.58	−9.50	1200	24.79 ± 0.71	M05
HD 34078	O9.5V	$4.77^{+0.41}_{-0.32}$	33.0	7.47	−9.50	800	24.64 ± 0.72	M05
HD 93028	O9V	5.05 ± 0.22	34.0	9.71	−9.00	1300	25.41 ± 0.71	M05
HD 152590	O7.5Vz	$4.79^{+0.33}_{-0.24}$	36.0	6.42	−7.78	1750	26.67 ± 0.71	M05
HD 93146	O6.5V((f))	$5.22^{+0.23}_{-0.25}$	37.0	9.97	−7.25	2800	27.50 ± 0.70	M05
HD 42088	O6.5Vz	5.23 ± 0.19	38.0	9.56	−8.00	1900	26.57 ± 0.70	M05
HD 93204	O5V((f))	$5.51^{+0.25}_{-0.20}$	40.0	11.91	−6.25	2900	28.55 ± 0.70	M05
HD 15629	O5V((f))	5.56 ± 0.18	41.0	12.01	−6.00	2800	28.79 ± 0.70	M05
HD 93250[a]	O3.5V((f +))	$6.12^{+0.25}_{-0.17}$	44.0	19.87	−5.25	3000	29.68 ± 0.70	M05

References. B12, Bouret et al. (2012); M17, Marcolino et al. (2017); C06, Crowther, Lennon & Walborn (2006); S08, Searle et al. (2008); M15a, Martins et al. (2015); A19, de Almeida et al. (2019); M15b, Mahy et al. (2015); M09, Marcolino et al. (2009); M12, Martins et al. (2012); M05, Martins et al. (2005). *Notes*. Homogeneous wind parameters are shown. Clumped models had the mass-loss rates re-scaled with a $\dot{M}/\sqrt{f}$ factor (see the text). [a]This star is mentioned as a prototype of the O3.5V class in Walborn et al. (2002). However, the Galactic O Star Catalogue of Maíz-Apellaníz et al. (2016) reports an O4IV(fc) classification.

Table 2. Stellar and wind parameters of SMC O and B stars analysed with CMFGEN models.

Star	SpT	$\log L/L_\odot$	$T_{\rm eff}$ (kK)	$R/R_\odot$	$\log \dot{M}$ ($\log \dot{M}_{\rm H\,\alpha}$)	V_∞ (km s^{-1})	$\log D$ ($\log D_{\rm H\,\alpha}$)	Reference
AzV 75	O5.5I(f)	5.94 ± 0.10	38.5	21.16	-5.80	2050	28.97 ± 0.20	B21
AzV 15	O6.5I(f)	5.83 ± 0.10	39.0	18.17	-5.96	2050	28.78 ± 0.20	B21
AzV 232	O7Iaf+	5.89 ± 0.10	33.5	26.39	-5.34	1350	29.30 ± 0.20	B21
AzV 83	O7Iaf+	5.54 ± 0.10	32.8	18.40	-5.64	940	28.77 ± 0.21	B21
AzV 327	O9.5II-Ibw	5.54 ± 0.10	30.0	21.99	-6.87	1500	27.78 ± 0.20	B21
MPG 355	ON2III	6.04 ± 0.10	51.7	13.17	-5.89	2800	28.92 ± 0.05	B13
AzV 77	O7III	5.40 ± 0.10	37.5	11.98	-7.38	1400	27.10 ± 0.20	B21
AzV 95	O7III((f))	5.46 ± 0.10	38.0	12.50	-6.90	1700	27.68 ± 0.20	B21
AzV 69	OC7.5III((f))	5.61 ± 0.10	33.9	18.67	-6.01	1800	28.68 ± 0.20	B21
AzV 47	O8III((f))	5.44 ± 0.10	35.0	14.40	-7.68	2000	27.00 ± 0.20	B21
AzV 307	O9III	5.15 ± 0.10	30.0	14.04	-8.32	1300	26.17 ± 0.20	B21
Azv 439	O9.5III	5.16 ± 0.10	31.0	13.30	-7.35	1000	27.01 ± 0.21	B21
AzV 170	O9.7III	5.14 ± 0.10	30.5	13.43	-8.32	1200	26.12 ± 0.21	B21
AzV 43	B0.5III	5.13 ± 0.10	28.5	15.20	-7.65	1200	26.82 ± 0.21	B21
AzV 177	O4V((f))	5.43 ± 0.10	44.5	8.81	-6.20	2400	28.45 ± 0.05	B13
AzV 388	O4V	5.54 ± 0.10	43.1	10.65	-6.52	2100	28.12 ± 0.05	B13
MPG 324	O4V	5.51 ± 0.10	42.1	10.79	-6.27	2300	28.41 ± 0.05	B13
MPG 368	O6V	5.38 ± 0.10	39.3	10.66	-6.93	2100	27.71 ± 0.05	B13
AzV 243	O6V	5.59 ± 0.10	39.6	13.37	-6.45	2000	28.21 ± 0.05	B13
AzV 446	O6.5V	5.25 ± 0.10	39.7	8.99	-7.90	1400	26.52 ± 0.06	B13
AvZ 429	O7V	5.13 ± 0.10	38.3	8.42	-7.90	1300	26.48 ± 0.06	B13
MPG 113	OC6Vz	5.15 ± 0.10	39.6	8.06	-8.52	1250	<25.83	B13
MPG 356	O6.5V	4.88 ± 0.10	38.2	6.34	-8.46	1400	<25.89	B13
MPG 523	O7Vz	4.80 ± 0.10	38.7	5.64	-9.22	1950	<25.25	B13
NGC 346-046	O7Vn	4.81 ± 0.10	39.0	5.62	-9.22	1950	<25.24	B13
NGC 346-031	O8Vz	4.95 ± 0.10	37.2	7.25	-9.22	1540	<25.20	B13
AzV 267	O8V	4.90 ± 0.10	35.7	7.43	-8.10	1250	26.23 ± 0.06	B13
AzV 461	O8V	5.00 ± 0.10	37.1	7.72	-9.00	1540	<25.43	B13
MPG 299	O8Vn	4.64 ± 0.10	36.3	5.33	-8.52	1540	<25.83	B13
MPG 487	O8V	5.12 ± 0.10	35.8	9.52	-8.52	1540	<25.96	B13
AzV 468	O8.5V	4.76 ± 0.10	34.7	6.70	-9.15	1540	<25.25	B13
AzV 148	O8.5V	4.84 ± 0.10	32.3	8.47	-8.70	1540	25.75 ± 0.06	B13
MPG 682	O9V	4.89 ± 0.10	34.8	7.73	-9.05	1250	<25.29	B13
AzV 326	O9V	4.81 ± 0.10	32.4	8.14	-9.15	1250	<25.20	B13
AzV 189	O9V	4.81 ± 0.10	32.3	8.19	-9.22	1250	<25.13	B13
MPG 012	B0IV	4.93 ± 0.10	31.0	10.20	-9.30	1250	<25.10	B13

References. B13, Bouret et al. (2013); B21, Bouret et al. (2021). Homogeneous wind parameters are shown ($f = 1.0$). Clumped models had the mass-loss rates re-scaled with an $\dot{M}/\sqrt{f}$ factor.

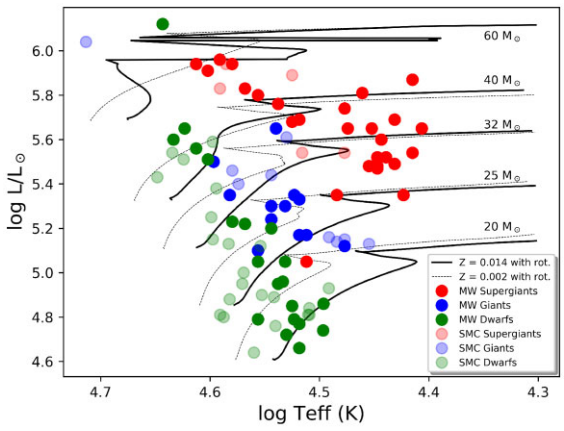

Figure 1. H-R diagram for the MW and SMC stars of our sample. Evolutionary tracks from Ekström et al. (2012) and Georgy et al. (2013) are indicated (see the text for more details). Note that I-III-V stars occupy different loci in the diagram.

UV spectra are notoriously important when studying the wind properties of hot massive stars because they contain several resonance doublets that provide the best diagnostics to derive the mass-loss rates and wind terminal velocities (not accessible in the optical). The sensitivity of the most important diagnostic wind line accessible to optical spectroscopy, namely Hα, is limited to winds with mass-loss rates greater than about 10^{-7} M$_\odot$ yr^{-1} (Marcolino et al. 2009). Winds 100–1000 times weaker can however be measured from the several UV resonance doublets and excited state wind lines, which is especially important for low-metallicity O stars, including those with weak winds (Martins et al. 2005; Marcolino et al. 2009).

In general, it is possible to constrain the intrinsic stellar luminosity by comparing the theoretical spectral energy distribution (SED) predicted by a model for a set of fundamental parameters (mostly $T_{\rm eff}$, $\log g$, R, $\dot{M}$, Z) to the observed multiwavelength data when extinction amounts and laws, as well as a distance, are taken into account. Distances to SMC stars are better constrained, in the sense that it can be considered they all share the same distance modulus of the SMC (e.g. DM $= 18.91 \pm 0.02$; Harries, Hilditch & Howarth 2003). They often suffer minimal extinction, leading to reliable estimates of stellar luminosities, radii and masses, crucial parameters in modelling their winds. This is not the case for Galactic stars, where distances are both

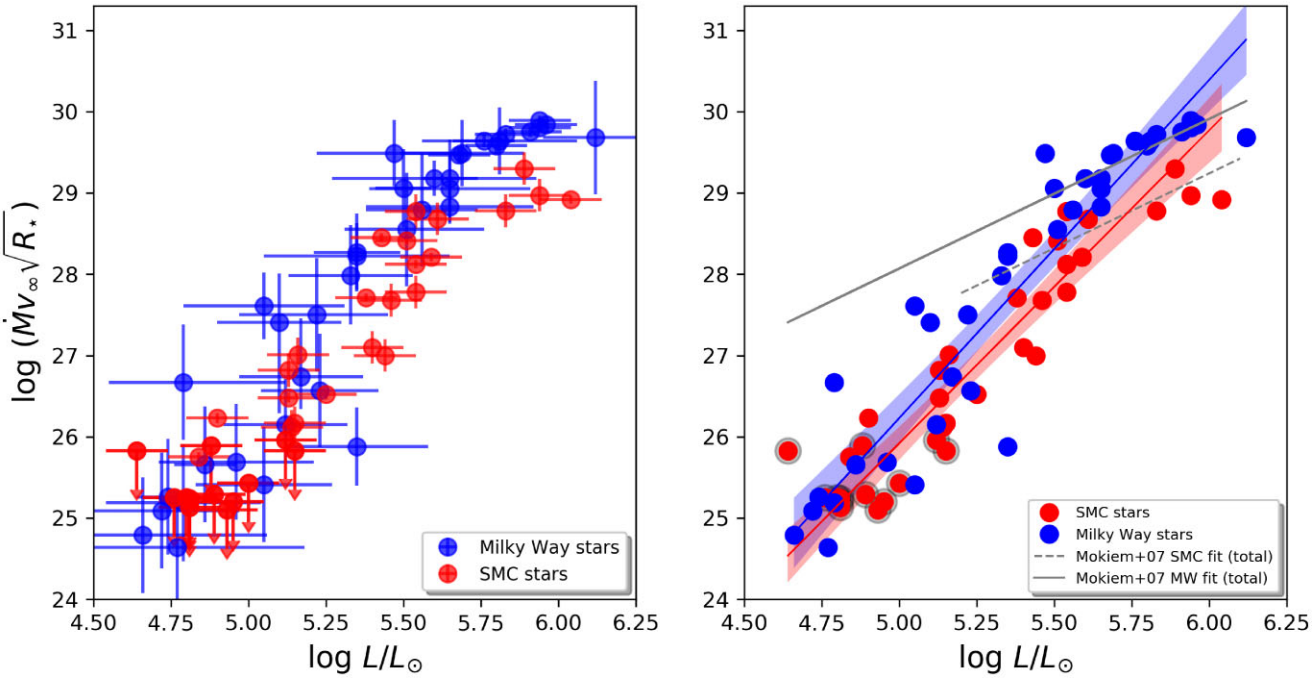

Figure 2. Wind momentum–luminosity relation of MW and SMC O and B stars. For clarity, the left-hand panel presents only the data and the respective error bars. The right-hand panel shows these same points along with regression lines and 2σ confidence bands (see the text for more details). Note that for $\log L/L_\odot \lesssim 5.4$ the MW and SMC data start to overlap. Only CMFGEN results based on a multiwavelength analysis are considered.

uncertain and varied, and extinction can be significant. In this case, either distances are adopted and the luminosities then derived from a SED fit, or the luminosities are fixed and spectroscopic distances can be inferred, which are then checked against observed parallaxes, if available. Although both strategies are reasonable and have been used for some stars in our sample (see e.g. Martins et al. 2012; de Almeida et al. 2019), uncertainties on quantities later used in this paper, namely stellar radii and luminosities, are notoriously higher for Galactic stars than for their SMC counterparts.

2.2 Consistent mass-loss rates: UV and optical

We will start with the wind momentum-luminosity relation, the WLR diagram: $\log D_{\rm mom} - \log L/L_\odot$, where L is the bolometric luminosity. By definition, $D_{\rm mom} = \dot{M}V_\infty\sqrt{R_\star}$. This quantity is called modified momentum and for theoretical reasons it is expected to correlate well with the luminosity (for more details, see Kudritzki & Puls 2000). In this relation, we used unclumped values for the mass-loss rates throughout this paper. If a model is clumped, the mass-loss rate is recomputed according to $\dot{M}_{\rm uncl} = \dot{M}_{\rm cl}/\sqrt{f}$ (f = micro-clumping parameter; see Bouret, Lanz & Hiller 2005).

In this section, we use results from models that successfully fitted ultraviolet and optical data at the same time, i.e. that refer to a single mass-loss rate for an object. The parameters used are listed in Tables 1 and 2. Mass-loss rate values between parentheses were obtained from the Hα line, independent of the UV. Stars with $\dot{M}$(Hα) are not used in this section (but see next section). We excluded the star HD 191423 of Mahy et al. (2015) from the analysis. This star has an atypical V_∞ of 600 km s^{-1} and very fast rotation, $V\sin I \sim 400$ km s^{-1}.

We present the WLR in Fig. 2. The left-hand panel shows only the data, and the right-hand panel presents them along with linear fits and confidence bands (more details below). To compute the uncertainty on the modified momentum, we need the uncertainties on $\dot{M}$, V_∞, and radius. However, they are not present in some of the works[1] quoted in Tables 1 and 2. Without V_∞ and radii errors, we adopted that the uncertainty on $D_{\rm mom}$ was purely due to the mass-loss rate uncertainty. Although not ideal, it is a reasonable assumption as both V_∞ and radius are usually known within much less than 50 per cent – i.e. the mass-loss rate uncertainty usually dominates (see e.g. Martins et al. 2005). However, when not available, the uncertainty on $\dot{M}$ was adopted to be a factor of 3. Regarding the luminosity, when not available, 0.25 and 0.10 dex of uncertainty were adopted, which are typical values for Galactic and SMC stars, respectively.

The fits to our MW and SMC data (Fig. 2, right-hand panel) were computed with Deming regression, which takes the uncertainties both in $D_{\rm mom}$ and L into account (Therneau 2018). For comparison, the WLR relations obtained by Mokiem et al. (2007) are also presented. We also computed confidence bands, which are displayed with 2σ as shaded regions. We note that the bands provided in the work of Mokiem et al. (2007) are 1σ and, therefore, much thinner than ours (see their fig. 4). All coefficients with the respective uncertainties are presented in Table 3. They will be explored later in Section 3.

In Fig. 2, we observe a clear relation between the modified wind momentum and the luminosity, as expected, in agreement with the radiatively driven wind theory (see Kudritzki & Puls 2000). This is observed for both the MW and SMC set. In general, the MW points are above the SMC ones, indicating a metallicity dependence.

[1]For example, Searle et al. (2008) do not provide errors on V_∞. This is also true in Mahy et al. (2015) for some objects of their sample, where V_∞ values from Prinja, Barlow & Howarth (1990) were adopted, and in Crowther et al. (2006). For some objects, mass-loss rates uncertainties are not reported either, neither radii uncertainties (see e.g. Martins et al. 2012; Mahy et al. 2015). On the other hand, some works provide all the necessary information (e.g. de Almeida et al. 2019), which we promptly used.

Table 3. Fit parameters to the MW and SMC data in Figs 2 (UV+optical; see Section 2.2) and 3 (emphasis on Hα; see Section 2.3).

WLR	Linear coeff. (α)	Slope (β)
Milky Way (UV+optical)	5.43 ± 1.28	4.16 ± 0.23
SMC (UV+optical)	6.67 ± 1.52	3.85 ± 0.29
Milky Way (Hα)	8.71 ± 1.64	3.60 ± 0.29
SMC (Hα)	6.67 ± 1.52	3.85 ± 0.29
Milky Way (Mokiem)	18.87 ± 0.98	1.84 ± 0.17
SMC (Mokiem)	18.20 ± 1.09	1.84 ± 0.19

Note. Fit parameters to the empirical data presented by Mokiem et al. (2007) is also shown (see their table 3).

However, there seems to be a metallicity degenerescence at low L, where MW and SMC points start to overlap.

We applied the Kolmogorov–Smirnov test to check whether the distributions of the MW and SMC stars in Fig. 2 could arise from the same population. We found a p-value of 0.006 57 for the null hypothesis that these two samples come from the same population, i.e. overall, we have a metallicity dependence on the wind strength, as the linear fits suggest. However, we also applied this test for the stars below $\log L/L_\odot = 5.2$. The corresponding p-value increases to 0.796, supporting a degenerescence.

Despite the facts aforementioned, in Fig. 2, we tagged a small subset of SMC stars (arrows in the left-hand panel and red symbols encircled in grey in the right-hand panel). These objects belong to the sample of Bouret et al. (2013). For them, the models fit well the observations but P-Cygni features are not conspicuous in the UV. The corresponding mass-loss rates were thus considered to be upper limits. Without these points, the angular coefficient of the fit to the SMC stars naturally decreases. This indicates that an analysis of more SMC objects with about the same luminosity values is urgently needed. The degeneracy might be weakened, removed or confirmed with more data points. Interestingly, two late O-type stars – AzV 267 (O8V) and AzV 148 (O8.5V) – present conspicuous wind profiles in the UV (see Bouret et al. 2013), allowing to derive specific values of their mass-loss rates. Both fall at low L and above some MW objects in the WLR, supporting the degeneracy. In fact, it is likely that the upper limits indicated in Fig. 2 are actually the true values because we observe a gradual decline of the wind profile intensities from early to late-type stars, which is reflected also on a gradual decline of the mass-loss rates, instead of jumps of some orders of magnitude (e.g. needed for a complete separation of the MW and SMC populations at low L).

We also note in Fig. 2 the discrepancy between our results (UV +optical) and the fits by Mokiem et al. (2007). These authors provided the most complete, empirical view of the wind metallicity dependence at that time. By analysing MW, SMC, and LMC data of several O and B stars, they found a clear evidence that MW stars have stronger winds than LMC stars, which, in turn, have stronger winds than SMC stars. Although *a priori* expected by the radiatively driven wind theory, this had never been shown quantitatively with such clarity (see their fig. 4).

Our data stand mostly below the fits by Mokiem et al. (2007). The slopes are very different. The main limitation of their study is the lack of modified momentum data for Magellanic Cloud stars with low luminosities. They constructed the empirical relations (linear fits) from the most luminous stars only, where $\log L/L_\odot \gtrsim 5.2$. Data points at lower L were upper limits that they neglected in the analysis. This is the reason for the interrupted dashed line in Fig. 2, for the SMC. The main cause of this issue is the difficulty in obtaining wind parameters with optical data. Hα is essentially in absorption at low L and often contaminated in stars close to nebular regions (see e.g. Ramachandran et al. 2019). We will come back to this question later in Section 5.

The CMFGEN measurements shown in Fig. 2 reveal an improved empirical relation with a reasonable number of stars in a large luminosity range (from dwarfs to supergiants). It updates and extends the results of Mokiem et al. (2007). It should be noted that Mokiem's relation is in general followed by the theoretical predictions of Vink et al. (2001), with only a small offset (∼0.2 dex, without clumping correction). This reasonable agreement strongly motivated works in the literature to use the theoretical recipe and the inferred Z dependence (e.g. Ekström et al. 2012). However, the results presented here show that this can be prone to errors, depending on the luminosity regime.

2.3 Inclusion of $\dot{M}$(Hα) results

In this section, we include mass-loss rates results based on optical – Hα, essentially. We consider them separately from the previous ones because some represent problematic measurements. There is a discrepancy between the $\dot{M}$ value obtained from Hα and from the UV for a few objects. That is, a single mass-loss rate does not fit the whole spectrum of an object, even when clumping and X-rays are taken into account (e.g. Martins et al. 2012). This is an open problem and will be discussed later in the paper. Some other results have $\dot{M}$ inferred from Hα and the fit to the corresponding UV spectra merely checked, with important discrepancies in some cases (e.g. Crowther et al. 2006). We include these Hα results for completeness, as they were also obtained with CMFGEN. In Table 1, they are denoted between parentheses. In some sense, our analysis anticipates the tendency of the WLR if the $\dot{M}$(Hα) values turn out to be preferred over $\dot{M}$(UV) ones for these objects in future works.

We proceed as follows: We keep data from the previous section where a single, robust mass-loss rate was obtained, i.e. when $\dot{M}(\mathrm{H}\alpha) \sim \dot{M}(\mathrm{UV})$. However, we add: (i) mass-loss rates based on fits to Hα and (ii) results for $\dot{M}$(Hα) that diverges from $\dot{M}$(UV). The samples used are from Martins et al. (2012) (O stars from Monoceros and NGC 2244), de Almeida et al. (2019) (some late O giants), Crowther et al. (2006) (early B supergiants only), and Searle et al. (2008) (early B supergiants only).

We present the WLR in Fig. 3. We first note that the MW stars are more scattered in this diagram, specially from mid- to low-luminosity values, in comparison with the previous figure. This reflects the effect of higher mass-loss rates from Hα in comparison with the UV rates for some objects (see Martins et al. 2012). When one favours Hα, the tendency is always to decrease the WLR slope.

Some of the features observed in Fig. 2 are also in Fig. 3: (i) We have more wind momentum as the luminosity increases, as expected; (ii) SMC massive stars present weaker winds compared to their MW counterparts; and (iii) the linear fits still indicate a severe departure from the fits of Mokiem et al. (2007) (see also Table 3). However, now the degeneracy at low L is not apparent. In order to better address these issues, we explore below the metallicity dependence of the mass-loss rate in a quantitative way.

3 EMPIRICAL METALLICITY DEPENDENCE

We can now analyse the metallicity dependence from the CMFGEN results presented above. We assume that $\dot{M} \propto \mathrm{Z}^m$ and that $v_\infty \propto \mathrm{Z}^n$,

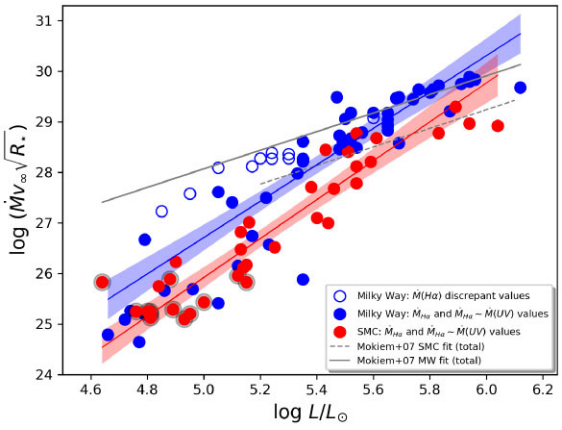

Figure 3. Same as Fig. 2 (right-hand panel), but preferring Hα over UV mass-loss rates measurements (see the text for more details).

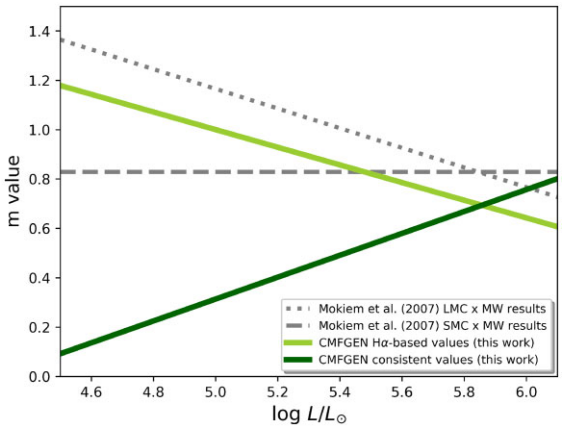

Figure 4. The metallicity dependence (m power) as a function of the luminosity – $\dot{M} \propto Z^m$.

with n fixed at 0.13, following Leitherer, Robert & Drissen (1992) (see however our discussion of the terminal velocities below). Therefore, with $\log D = \log(\dot{M}v_\infty\sqrt{R_\star})$, we can write the difference:

$$\Delta \log D \equiv \log D_{\rm MW} - \log D_{\rm SMC} = (m+n)\log\frac{Z_{\rm MW}}{Z_{\rm SMC}}. \quad (1)$$

Our fits for the MW and SMC provide (see Figs 2 and 3)

$$\log D_{\rm MW} = \beta_{\rm MW}\log L/L_\odot + \alpha_{\rm MW}, \quad (2)$$

$$\log D_{\rm SMC} = \beta_{\rm SMC}\log L/L_\odot + \alpha_{\rm SMC}, \quad (3)$$

where β and α are the angular and linear coefficients, respectively (see Table 3). Combining the equations, we can compute m as a function of the luminosity through

$$m = \frac{(\beta_{\rm MW}-\beta_{\rm SMC})\log L/L_\odot + (\alpha_{\rm MW}-\alpha_{\rm SMC})}{\log Z_{\rm MW}/Z_{\rm SMC}} - n. \quad (4)$$

In Fig. 4, we use equation (4) on the empirical results presented in the last sections. We adopt $Z_{\rm SMC} = 1/5\ Z_{\rm MW}$. For comparison, we also display the results by Mokiem et al. (2007), regarding SMC x MW and also LMC x MW. With our consistent values for the wind momenta, the m exponent increases with luminosity, a fact that is apparent from Fig. 2 – where the MW and SMC points start to disentangle. In contrast, a very weak Z dependence is revealed by the fact that $m \to 0$ at low L.

If we take into account the Hα-based D values, we do not observe the same trend. At low L, the lines separate even further – $\dot{M}$(Hα) > $\dot{M}$(UV), increasing m. However, the consistent values are the ones to be followed. The Hα-based values are shown here only for completeness (see Section 5).

The m value obtained by Mokiem et al. (2007) is 0.83, which is explicit in Fig. 4 as an horizontal dashed line (SMC x MW). Such a value is only perceived by our results at the high-luminosity end. At $\log L/L_\odot = 5.75$, the value chosen by Mokiem et al. (2007) to compute m, our results indicate a milder dependence, $m \sim 0.6$. For the LMC x MW, the data explored by Mokiem et al. (2007) suggest that the Z dependence gets stronger at low L, if extrapolated. But there, their results are uncertain.

Overall, the present analysis suggests that the metallicity dependence of O stars is better seen at high luminosities. There, the different relations diverge less. Regarding our data, for $\log L/L_\odot \gtrsim 5.4$, where we see start to see a clear separation of MW and SMC points in Fig. 2, the m values fall in the interval 0.5−0.8. Hence, above this threshold, we suggest $\dot{M} \propto Z^{0.5-0.8}$ as a reasonable, realistic relation.[2]

On the other hand, the weaker $\dot{M}(Z)$ dependence found at low luminosities ($m \to 0$) deserves to be investigated in future studies, with a larger sample. If such stars indeed loose about the same amount of mass per year regardless the environment (Z), there are likely evolutionary consequences (e.g. angular momentum, mixing). As low L means less massive, this problem would affect the majority of O and B stars, as required by an initial mass function (IMF) distribution.

4 TERMINAL VELOCITIES

In this section, we analyse the terminal velocities (V_∞) of our sample stars to check for a possible metallicity dependence. Some theoretical calculations indicate that V_∞ should scale with metallicity as $V_\infty \propto Z^n$. For example, Leitherer et al. (1992) computed a multiple linear regression to their set of radiatively driven wind solutions for several theoretical stars in the H-R diagram, of different metallicities, obtaining $\log V_\infty = 1.23 - 0.3\log(L/L_\odot) + 0.55\log(M/M_\odot) + 0.64\log T_{\rm eff} + 0.13\log(Z/Z_\odot)$. The last term implies $n = 0.13$, a value that is widely used in the literature. On the other hand, Krtička & Kubát (2018) found from hydrodynamical calculations a metallicity dependence for the mass-loss rate ($\dot{M} \propto Z^{0.59}$), but that the average values of V_∞/V_{esc} (V_{esc}, the escape velocity) for stars in the LMC, SMC, and MW were similar, in contrast to what was found by Leitherer et al. (1992). More recently, Björklund et al. (2021) inferred a negative but still shallow n value (-0.10 ± 0.18) and Vink & Sander (2021) inferred $n = 0.19$.

Using spectroscopic observations, V_∞ can be measured with or without atmosphere models. Well developed P-Cygni profiles in the UV can be used for a direct determination by using the bluest wavelength of zero intensity (i.e. $V_{\rm black}$) or *narrow absorption components – NACs* (see Prinja et al. 1990). With models, detailed fits to the whole absorption part of the P-Cygni profiles provide the measurements, with a depth dependent turbulence included. In general, these two methods agree very well within a few per cent (see Crowther et al. 2006, and references therein).

[2]We remind that we have used Deming regression, which takes the errors both in the modified momenta and luminosities properly into account when fitting the data. If a simple linear regression is applied, m in the interval 0.6−1.2 is obtained for $\log L/L_\odot \gtrsim 5.4$.

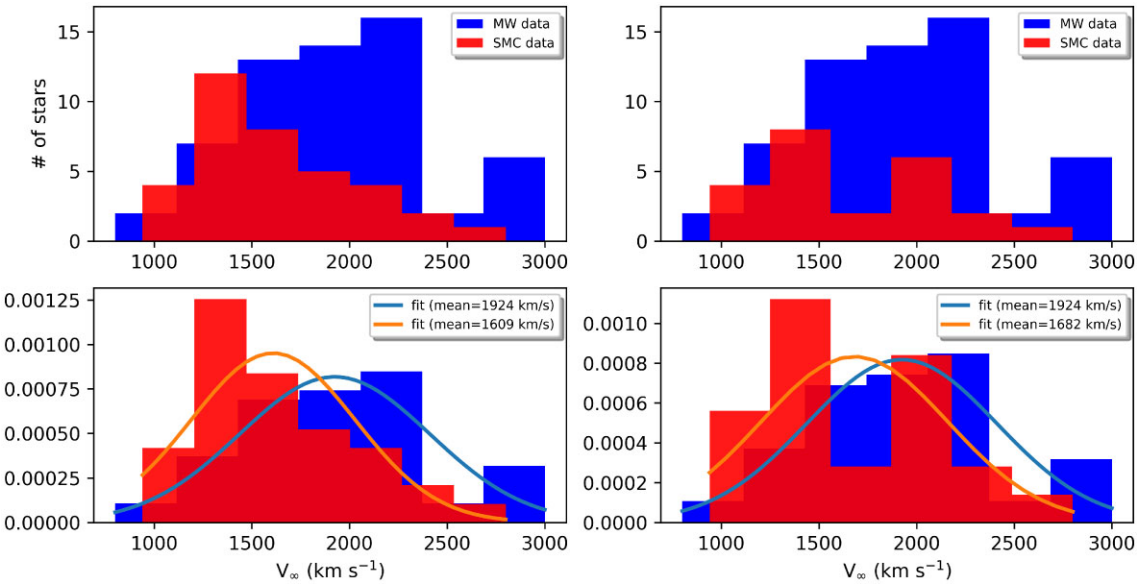

Figure 5. Terminal velocity distribution of our sample of O and B stars in the MW and SMC. The left-hand panels include all our data. The right-hand panels exclude SMC stars without conspicuous wind profiles in Bouret et al. (2013) (see the text for more details).

In our sample, most measurements were obtained directly from the comparison between observed and synthetic P-Cygni profiles in the UV. In some occasions, values from the literature were adopted for V_∞. Nevertheless, the fit quality to diagnostic lines is always checked and adjustments are made, when necessary. For example, Crowther et al. (2006) used $V_{\rm black}$ values from previous works and Searle et al. (2008) used the UV-based results of Prinja, Massa & Searle (2005) as input for V_∞, getting reasonable fits to some UV profiles.[3]

Bouret et al. (2013) achieved satisfactory fits to the wind profiles in their SMC sample, obtaining V_∞ within $\pm$ 100 km s^{-1}. However, for stars without or with undeveloped P-Cygni profiles, V_∞ measurements becomes challenging, sometimes impossible. In such cases, Bouret et al. (2013) adopted terminal velocities of MW stars of similar spectral types from Kudritzki & Puls (2000) and applied a $V_\infty \propto Z^n$ scaling, using $n = 0.13$ (Leitherer et al. 1992) and the SMC metallicity. These objects can be identified in Table 2 when the modified momentum value informed is an upper limit. Although the observed profiles were well reproduced, the reliability of these V_∞ values is questionable. Due to this fact, we will present below an analysis with and without these sources.

We present in Fig. 5 histograms of the terminal velocities listed in Tables 1 and 2. By taking into account all data (left-hand panels), a metallicity dependence is suggestive. Indeed, a Kolmogorov–Smirnov test to check whether these data come from a same population returns a p-value of 0.002 215. Normal fits to the two distributions return $\bar{V}_\infty(SMC) = 1609$ ($\sigma_{\rm SMC} = 419$ km s^{-1}) and $\bar{V}_\infty(MW) = 1924$ km s^{-1} ($\sigma_{\rm MW} = 488$ km s^{-1}). If we use these mean velocities and assume that $V_\infty \propto Z^n$, we can roughly estimate that $n \sim 0.11$.

Similarly, but neglecting the SMC stars in Bouret et al. (2013) that do not have conspicuous wind profiles, we obtain that $\bar{V}_\infty(SMC) = 1682$ km s^{-1} ($\sigma_{\rm SMC} = 478$ km s^{-1}). In this case, however, we infer $n \sim 0.08$ and the p-value of the Kolmogorov–Smirnov test increases to 0.1348, weakening the evidence.

The use of this Z^n scaling is of course valid when we consider the same physical parameters (luminosity, mass, temperature) except for the environment metallicity (Z). Despite using mean values from stars with different physical parameters, it is interesting that the values obtained above are relatively close to the theoretical value inferred by Leitherer et al. (1992), $n = 0.13$. The data indicate that the stellar winds of O and B stars in the SMC are roughly ∼15 per cent weaker if compared with the O and B stars in the MW, on average.

A detailed analysis of V_∞ taking into account data of several O and B stars in the MW, LMC, SMC, M31, M33, and IC 1613 was presented by Garcia et al. (2014). It was the first detailed study of terminal velocities that included massive stars beyond the Magellanic Clouds. These authors reported a Z dependence, but with IC 1613 stars occupying about the same loci than Magellanic Cloud stars in the V_∞–$T_{\rm eff}$ diagram (see Garcia et al. 2014; Bouret et al. 2015, for a discussion of the actual metallicity of the IC 1613 galaxy).

In Fig. 6, we display our data in the V_∞–$T_{\rm eff}$ plane, as done by Garcia et al. (2014). These authors explored in detail the complexity of the V_∞/V_{esc} distribution, showing that it can be very uncertain to estimate V_∞ from V_{esc} from the canonical 2.65 ratio (Kudritzki & Puls 2000). Here, we refrain from repeating a V_∞/V_{esc} analysis. Instead, we use the linear fits in Fig. 6 to provide a rough estimate for the n power in the Z dependence.

Using that $V_\infty = \beta T_{\rm eff} + \alpha$ with the respective coefficients from the MW and SMC fits (SMC – all data: $\alpha = -984.1$, $\beta = 71.2$; MW: $\alpha = -646.6$, $\beta = 76.72$; SMC – neglecting data: $\alpha = -971.2$, $\beta = 72.2$) and that $V_\infty \propto Z^n$, we can write

$$\log\left(\frac{Z_{\rm MW}}{Z_{\rm SMC}}\right)^n = \log\frac{\beta_{\rm MW}T_{\rm eff} + \alpha_{\rm MW}}{\beta_{\rm SMC}T_{\rm eff} + \alpha_{\rm SMC}}. \quad (5)$$

From this expression, considering the complete sample, we infer n values between 0.16 and 0.22, for the $T_{\rm eff}$ interval ∼40–30 kK, where most points are. Neglecting the same aforementioned SMC stars from Bouret et al. (2013), we infer infer a slightly lower range of n values, namely 0.14−0.20.

[3]We note that lines from certain ions were not properly reproduced in their study due to absence of X-rays in the models.

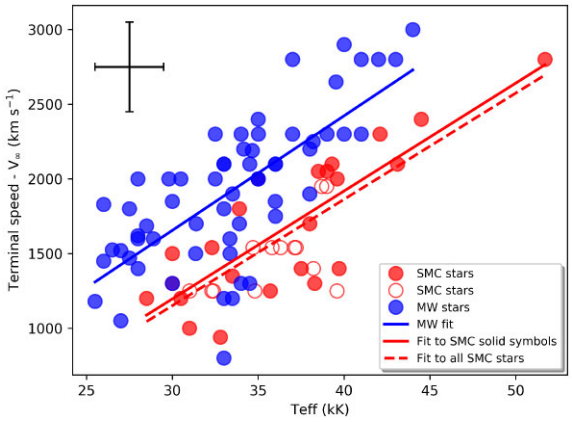

Figure 6. Terminal velocity versus effective temperature for our sample of O and B stars in the MW and SMC. In general, MW stars possess larger velocities if compared with SMC stars. Representative error bars are shown: 2000 K in temperature and 300 km s^{-1} in velocity. SMC stars represented by open circles do not have conspicuous wind profiles (see the text for more details).

We conclude that the terminal velocity dependence on Z that can be inferred from the CMFGEN results – $V_\infty \sim Z^n$ – has n in the range 0.08−0.22, or approximately, $n \sim 0.1-0.2$. A low exponent seems to be appropriate for V_∞ scaling in different environments, supporting Leitherer et al. (1992).

The results above illustrate the need for an analysis of a larger sample of stars. In particular, very weak wind profiles should be used with caution and realistic error bars should be provided. Moreover, pure absorption lines or doubtful wind profiles should be neglected. This would help improve the statistics considerably.

5 DISCUSSION

We now discuss our findings, caveats, as well as other results in the literature.

5.1 Hα uncertainties

Given the importance of the degeneracy question at low L, it is appropriate to discuss the mass-loss rates obtained from Hα measurements. The modified wind momentum-luminosity relation gets more scattered because we favored Hα over UV measurements, when discrepant, changing the linear fit (see Fig. 3).

We remind that Hα-based measurements are not free from problems and sometimes they can be very uncertain at mid- and low luminosities (giants and specially dwarfs). From an observational point of view, Hα data are relatively easy to obtain, specially for bright objects (low exposure times), where it is in emission, allowing fairly easy mass-loss rate determinations. It is no surprise that the first modern quantitative spectroscopic studies in the literature were optical-based, favoring OB supergiants.[4] Moreover, hydrogen is a simpler atom to treat than CNO and Fe-group ions in atmosphere models. These facts provide a bias towards Hα measurements and bright objects.

However, Hα can be mostly in absorption in O giants and dwarfs. The determination of the mass-loss rate in such cases is based on the wind emission that fills the core of the photospheric line. This can be very uncertain, depending on the object/sample. For example, nebular emission from Balmer lines is common around young objects (e.g. in dwarfs). Some cases observed go from weak to strong central emission superposed on the Hα absorption profile. In some other cases, one cannot be sure whether there is a weak nebular or a wind contribution to the observed profile, or both. Line-filling from a contamination of a companion star have been also claimed as a possibility in the literature. Such difficulties have been reported in different works and can hinder a reliable mass-loss rate determination (see e.g. Ramachandran et al. 2019; Ramírez-Agudelo et al. 2017).

Of course, not everything can be assigned to observational issues. There are cases where Hα seems free of contamination and the models cannot fit it simultaneously with the wind diagnostics in the UV. Therefore, it is indeed possible that the models are incomplete and inadequate for some objects. Assuming that this is true, on the other hand, it is puzzling that for every luminosity class we have examples where models successfully fit the observed profiles, from the ultraviolet to optical.

In brief, we have discussed the impact (Section 2.3) and uncertainties of the Hα mass-loss rate measurements. However, *consistent rates* – that successfully match the UV and optical wind diagnostic lines – are the ones to be taken into account. Obviously, the discrepancies found in some objects still deserve investigations. However, until this question is settled, there is no reason to give more weight to Hα over UV $\dot{M}$ measurements.

5.2 UV uncertainties

Detailed analyses of UV spectra with CMFGEN provide a way to determine mass-loss rates and also terminal velocities, which are necessary to compute the modified momentum $D_{\rm mom}$ ($= \dot{M} V_\infty \sqrt{R_\star}$). However, how robust are these mass-loss rates? In particular, how certain can we be about the possible degeneracy implied by Fig. 2?

First, we remind that the rates in Fig. 2 are consistent. That is, the models present a reasonable fit to the UV and optical spectra for the sample stars. However, it is a fact that some CMFGEN models fail to fit these two spectral regions simultaneously for a couple of stars, as previously mentioned. This raises the question whether CMFGEN really grasp the essential physics present in the winds of O stars or provide only rough mass-loss rates in some cases.

5.2.1 *Clumping*

Radiatively driven winds are far from being homogeneous (Owocki, Castor & Rybicki 1988). Line instability cause strong shocks within a stellar wind, generating X-rays and a variety of effects on the outflow. The winds present time dependent structures, with strong density (clumping), temperature, and velocity variations. In CMFGEN, only an approximate treatment is made to incorporate the effects of X-rays and clumping. In general, the clumps are assumed to be optically thin (micro-clumping) and the inter-clump medium is void.[5]

However, it has been shown that clumps can become easily optically thick in strong UV wind lines. The effects of clumps

[4]It is worth noting that the UV and optical diagnostics usually provide a single mass-loss rate for these objects.

[5]The presence of clumping enhances recombinations, making ρ^2-sensitive lines stronger compared with the ones from homogeneous models. Therefore, clumped models mass-loss rates must be decreased by a factor of $1/\sqrt{f}$ in comparison with homogeneous models to fit the observations (see Bouret et al. 2005).

of arbitrary optical depths (from thin to thick) and of an inter-clump medium on UV line profiles have been explored recently by Sundqvist & Puls (2018) (see also references therein). They incorporated optically thick effects (porosity and vorosity) in the FASTWIND code through the use of effective opacities. These authors explored two UV resonance lines, from N v and P v, and found that they get weaker compared with the ones from optically thin clump models. This indicates that mass-loss rates from models taking into account micro-clumping are underestimated.

In the context of this work, we remind that: (i) we corrected the mass-loss rates from CMFGEN models with (micro-) clumping upwards by a $1/\sqrt{f}$ factor. That is, we used only homogeneous values in our plots. For $f = 0.1$, for example, the correction is about a factor of 3; (ii) the changes on the UV line intensities found by Sundqvist & Puls (2018) from optically thin *versus* optically thick models are not huge (see their fig. 4). Although not quoted by these authors, we estimate that the mass-loss rate corrections with the optically thick clumping effects included are below a factor of 10. Hence, although the WLRs obtained in this paper can be somehow modified with a more realistic description of clumping, we speculate that the impact on the mass-loss rates will be, to some extent, compensated by our correction from micro-clumping to homogeneous rates.

The question above will be only settled when a large number of objects is analysed relaxing the micro-clumping assumption, preferably using multiwavelength diagnostics. A limitation of the work by Sundqvist & Puls (2018) is that they explored only UV profiles from ζ Pup like models, i.e. early-type stars. Therefore, we lack a view of the optically thick effects on UV lines in different type of objects, e.g. of low luminosities and of different metallicities. It remains also to be explored whether the effects will solve the discrepant mass-loss rates measurements from the UV and Hα made by CMFGEN in a couple of objects (see e.g. Martins et al. 2012).

We note that new alternative approaches to this problem start to emerge. Flores & Hillier (2021) for example, represent clumping by dense spherical shells with the CMFGEN code. The opacity naturally follows from the density variations within the wind. Thus, the interclump medium and arbitrarily optical depths are automatically taken into account. Flores & Hillier (2021) obtain a mass-loss rate 40 per cent higher than the micro-clumping approach, for the supergiant AzV83 (O7Iaf +). It remains to be seen whether this trend will persist for stars of different spectral types and luminosity classes.

Another major concern regarding clumping is its metallicity dependence. For example, if the filling factors[6] vary with Z, different mass-loss corrections are expected (Sundqvist 2013). The WLR for the MW and Magellanic Clouds stars would then change in a significant way. Currently, this is an open question.

Interestingly, there are some works in the literature that favour a Z-independent view of clumping. For example, Marchenko et al. (2007) presented time-resolved spectroscopy of three SMC Wolf–Rayet stars with the ESO-VLT-UT2 8-m telescope, finding evidence of small-scale structures moving within the outflow. The measured properties of these clumps – velocity dispersion, acceleration and emissivities – were found to be similar to the ones found in Wolf–Rayet stars of the MW. In addition, Lépine & Moffat (2008) monitored optical lines of a small sample of Galactic O and W-R stars, reporting similar *lpv* patterns for all objects. They concluded that 'stochastic wind clumping is a universal phenomenon in the radiation-driven, hot winds from all massive stars, with similar clumping factors in all stages of mass depletion'. Hence, the results of both studies – Marchenko et al. (2007) and Lépine & Moffat (2008) – naturally lead to the conclusion that clumping is similar in stars of different evolutionary stages, regardless the environment. Unfortunately, we lack similar studies confirming this view, for a larger sample of stars.

It is also worth noting that there is no indication that the filling factors and the onset of clumping are drastically different in MW and Magellanic Cloud objects, with the usage of micro-clumping in CMFGEN models. If there is a Z dependence, it is subtle to the point of not being perceived by such standard analyses.

5.2.2 *Weak winds*

Mass-loss rates inferred for low-luminosity O stars were found to be much lower than predicted by theory (e.g. Martins et al. 2005; Marcolino et al. 2009; Puls et al. 2008). For example, UV line profiles obtained from atmosphere models match the observed ones in O8-9V stars when mass-loss rates are typically 10^{-9} $M_\odot$ yr^{-1}. For these same type of objects, theory predicts roughly 10^{-7} $M_\odot$ yr^{-1}. This problem challenges our understanding of the winds of these objects. In the context of this work, if there is an issue with the atmospheric measurements and the winds are not weak – e.g. they are as predicted by theory (Vink et al. 2001) – our results at low L are called into question.

In the last decade, several works in the literature approached the weak wind problem. Lucy (2010), using a Monte Carlo technique, obtained theoretical mass fluxes somewhat compatible with the ones observed in late-type O stars, about 1.4 dex lower than Vink et al. (2001). On the other hand, by updating their work, Vink et al. (2001) and Muijres et al. (2012) reported that their models failed to produce winds at low luminosities due to a lack of Fe V lines, which possibly indicates the need of other mechanisms to help the wind driving.

Vilhu & Kallman (2019) suggested that the solution is related to the velocity span within a wind clump (using a velocity filling factor FVEL = 0.1). When taken into account, the radiative force was modified and the mass-loss rates observed for late-type O stars (obtained by atmosphere models) were matched by their models. Notwithstanding, the physical reason for the specific value of the velocity filling factor used remained unclear. Also unclear was the fact that this effect was not needed for brighter objects (FVEL = 1).

Sundqvist et al. (2019) provided mass-loss rates from hydrodynamical simulations that used a radiative force computed from co-moving NLTE radiative transfer solutions, in a self-consistent way. For parameters close to that of an O7V star, the rate obtained was about 9 times lower than predicted by Vink et al. (2001), a tendency towards weak winds but not a solution. New simulations by Vink & Sander (2021) and Björklund et al. (2021), which we discuss later in the paper, maintain relatively high mass-loss rates for a typical late O-type star and therefore the weak wind problem.

An interesting solution was recently proposed by Lagae et al. (2021), which carried out hydrodynamical simulations that took into account the line-deshadowing instability (LDI). The LDI naturally creates a very structured wind, with drastic variations in velocity, density and temperature. For low-luminosity O stars, their simulations show that most of the outflowing gas is shocked, with temperatures well above 10^5 K. The line profiles computed with these models were weaker than the ones from homogeneous models,

[6]One should be careful about the nomenclature. In our notation, we have the clumping volume filling factor $f \leq 1.0$. In the literature, the inverse is often called the clumping factor ($D = 1/f$).

for a same mass-loss rate. This indicates that the mass-loss rates are underestimated if the shocked region is not taken into account. That is, all current UV based rates from atmosphere models are questioned at low luminosities.

In order to confirm this scenario, the calculation of the amount of X-rays emitted from their models and a comparison with the observations is necessary. If about ∼70 per cent of the wind volume of an O dwarf has temperatures about 10^5-10^7 K, as found by these authors, a large contribution to the integrated X-ray emissivity and thus total X-ray emission, is expected. Similarly, we expect less X-ray emission from their O supergiant model, as the volume fraction of the shocked, hot wind is only about 7 per cent and on average its temperature is below 10^5K. A priori, X-ray observations seem to be in contrast with these considerations unless the different gas densities in these two cases counteract the very different volumes and temperatures of the hot gas. It is known that for O stars log $L_X/L_{BOL} \sim -7.0$ (see e.g. Sana et al. 2006; Oskinova, Feldmeier & Hamann 2006). About the same value is observed in O dwarfs and supergiants. High- (low-) luminosity stars having high (low) L_X.

In this same context, we note that some X-rays results support the reality of weak winds, with mass-loss rates as low as the UV measurements (e.g. Cohen et al. 2014; Doyle et al. 2017). Interestingly, the work of Huenemoerder et al. (2012) presents an X-ray based mass-loss rate of about 2.0×10^{-9} $M_\odot$ yr^{-1} for the O9.5V star μ Col. Although the authors claim that the wind is not weak, this value is not far from the ones found for other late-type O stars (see e.g. ζ Oph in Marcolino et al. 2009). Also, the value predicted from theory (Vink) for this star is 1.1×10^{-8} $M_\odot$ yr^{-1}, which means a considerable difference compared with the observed value (of about 0.8 dex).

Despite several attempts, there is not yet a solution for the weak wind problem. Some of the works mentioned above decrease the mass-loss rates in comparison with Vink et al. and even match the very low rates measured by atmosphere models, but there is no consensus so far. In any case, there are no clear evidences to disregard atmosphere model results at low L, as the ones presented here. Some theoretical calculations have shown that very low rates are plausible.

5.3 Other measurements and techniques in the literature

Recently, Ramachandran et al. (2019) presented an analysis of 320 stars at the SMC: 297 B stars and 23 O stars. The authors used the Potsdam Wolf–Rayet code (PoWR) to model their spectra and derive stellar and wind parameters. For the majority of the sample, $\dot{M}$ was obtained as an upper limit from Hα. Given the location of the observed stars in the SMC – the supergiant shell SMC-SGS1 – severe ISM contamination remained in this line even after the sky subtractions performed. This is an example of how uncertain Hα can be in some cases. We do not consider their Hα measurements here.

For nine objects in their sample, low-resolution (6–7 Å) *IUE* spectra are available and were used. One supergiant – identified as SMCSGS-FS 310 – also has a *HST* (*Hubble Space Telescope*) high-resolution spectrum (resolving power $R = 18\,000$). The uncertainties reported by Ramachandran et al. for the mass-loss rates and terminal velocities are relatively small, ±0.2 dex and about 10 per cent, respectively. We remind that all UV results from CMFGEN used in the previous sections are based on high-resolution data.

In Fig. 7, we present the WLR diagram of the nine stars analysed with the PoWR atmosphere code by Ramachandran et al. (2019), the ones with UV data, along with the linear fit for our (CMFGEN) SMC sample (see Fig. 2 and Table 3), extrapolated down to log $L/L_\odot \sim$ 4.3. Nominal values for the mass-loss rates from their table B.2 are used, since they are independent of the adopted clumping parameters (see Ramachandran et al. 2019).

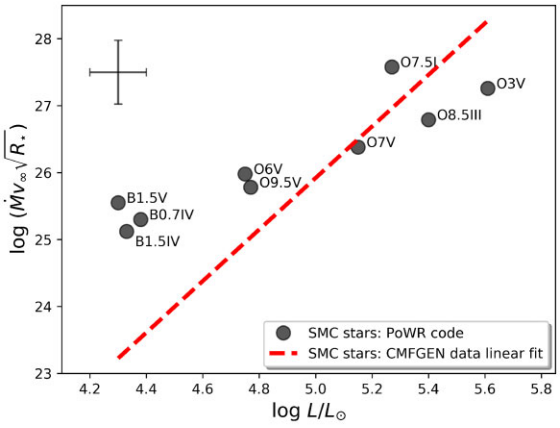

Figure 7. WLR diagram for nine SMC stars analysed with the PoWR code. The linear fit is based on our CMFGEN data for the SMC stars. Representative error bars and spectral types are indicated. Note the good agreement for the O stars and that B stars stand above the fit (see the text).

The B stars, which are cooler than all stars considered in our CMFGEN sample (at low L), stand above the fit. A possible explanation for this behaviour is bi-stability. The temperatures of the B1.5V, B1.5IV, and B0.7IV stars are 22, 20, and 27 kK, respectively (Ramachandran et al. 2019). From about 27.5 to 22.5 kK, the mass-loss rates and therefore log D, are expected to increase by some factors due to the bi-stability phenomenon (Vink et al. 2001).

On the other hand, there is good agreement for the O stars. This fact supports the physical parameters obtained with CMFGEN and the metallicity trend discussed in Section 2. We remind however that the determination of accurate stellar wind parameters for metal-poor late-type O (or early B) dwarfs from low-resolution UV spectra is challenging. Both characteristics, spectral-type and low-Z environment, combine to produce wind profiles that are very weak to be seen even in high-resolution data. In this context, it would be reassuring to have a PoWR re-analysis of Ramachandran's sample based on new high-resolution spectroscopic observations.

Regarding the LMC, the VLT-FLAMES TARANTULA survey resulted in several papers on the physical and chemical properties of O and B stars. Here, we briefly discuss the papers by Ramírez-Agudelo et al. (2017) and Sabín-Sanjulián et al. (2017), which addressed stellar wind parameters. Both used optical data.

Ramírez-Agudelo et al. (2017) analysed a sample of 72 giants, bright giants and supergiants massive stars at the LMC with an automatic fit procedure using FASTWIND (PIKAIA). About 40 per cent of their sample, the low L stars, have only upper limits on $\dot{M}$. These stars were neglected in their WLR analysis and linear fits were provided only considering stars with log $L/L_\odot > 5.0$, in contrast to our results. The fits are close to the ones of Mokiem et al. (2007) for the LMC.

Regarding the population of dwarfs in the LMC, Sabín-Sanjulián et al. (2017) analysed 105 O and B stars, also through a robust automatic fit method (IACOB-GBAT). Given the low-metallicity content and luminosity of dwarfs, again only upper limits on mass-loss rates could be provided for the latest spectral-type stars (log $L/L_\odot \leq 5.1$). Again, the linear fits were provided considering only bright objects, log $L/L_\odot > 5.1$.

Although we do not address LMC stars in the present paper, we remind that our fits are steeper for the SMC and MW in comparison

with Mokiem's relations. We anticipate that an analysis of LMC stars data from CMFGEN models will be just in marginal agreement with Mokiem's, Ramírez-Agudelo et al. (2017), and Sabín-Sanjulián et al. (2017) results, at high luminosities.

In these works, the terminal velocities are not measured directly. In the absence of UV data, they are usually estimated from the escape velocity through the relation $v_\infty/v_{esc} \sim 2.6$, scaled to the LMC or SMC metallicity. As discussed before, Garcia et al. (2014) show that the use of this specific value may be prone to substantial errors. This is a source of uncertainty for the (already) upper limits on $\log D$ of Sabín-Sanjulián et al. (2017) and Ramírez-Agudelo et al. (2017) for the low-L stars.

In short, optical-only measurements of mass-loss rates of low-luminosity O and B stars in Magellanic Clouds should be considered with caution. The $\log D \times \log L/L_\odot$ trend at low Ls is better addressed with our results (and of Ramachandran et al. 2019), based on fits to UV and optical spectra.

5.3.1 *Bow-shock measurements*

Recently, a very promising technique based on bow shocks to infer $\dot{M}$ has been explored in the literature (e.g. Gvaramadze, Langer & Mackey 2012; Henney & Arthur 2019; Kobulnicky, Chick & Povich 2019). The winds of massive stars can produce shocks when encountering the ISM medium, producing arc-shaped emission that can be successfully detected and imaged at infrared wavelengths (e.g. at 24 μm). The mass-loss rate can be expressed in terms of the physical properties of this shocked region (e.g. dust emission coefficient, infrared surface brightness). This technique is considerably diverse than quantitative multiwavelength spectroscopy, since no comparison with observed spectra or other observable is done. Nevertheless, it is of extreme importance as an independent check of the mass-loss rates obtained so far from other techniques.

We focus here on the latest work by Kobulnicky et al. (2019), given the large sample analysed homogeneously. These authors obtained mass-loss rates for 67 galactic O and B stars with bow-shock nebulae. The results were compared with the predictions of Vink et al. (2001) in the $\log \dot{M} \times \log T_{\rm eff}$ and WLR diagrams. Overall, an average discrepancy with the predicted values (Vink) of -0.43 dex was inferred for stars with $T_{\rm eff} > 25$ kK, with a large dispersion of 0.64 dex (see their fig. 9). Regarding the WLR diagram, a systematic offset of about 0.4 dex was also observed, below the predicted relation. That is, in general, the mass-loss rates or wind strengths derived were less than predicted by the radiatively driven wind theory, which is followed closely by the relations of Mokiem et al. (2007).

We present in Fig. 8 the linear fits obtained from CMFGEN and Mokiem's MW data, along with the bow-shock measurements of Kobulnicky et al. (2019). The error bar is representative and assumes an uncertainty of 40 per cent for the mass-loss rate, as estimated by Kobulnicky et al. (2019), neglecting errors on the wind terminal velocity and stellar radius. To avoid low effective temperatures ($T_{\rm eff} \lesssim 25$ kK) and thus the onset of bi-stability, only O and B stars with spectral types earlier than B0 are displayed.

Most points fall between the CMFGEN and Mokiem's relations. There is marginal agreement with the results from CMFGEN for only about 12 objects out of 46 (about 25 per cent of their sample). These measurements suggest a less steep WLR and the removal of the degeneracy mentioned in Section 2. However, there are some points that deserve to be discussed.

First, we note that there is a considerable scatter for specific luminosity ranges/spectral classes in Kobulnicky et al. results. Regarding

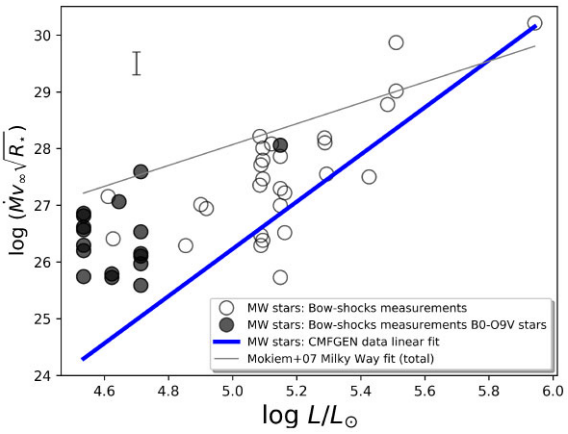

Figure 8. WLR diagram for MW stars, adding measurements based on bow-shocks by Kobulnicky et al. (2019). Linear relations from the results obtained with CMFGEN and from Mokiem's work are displayed (see Section 2). B0-09V stars are shown with filled circles (see the text).

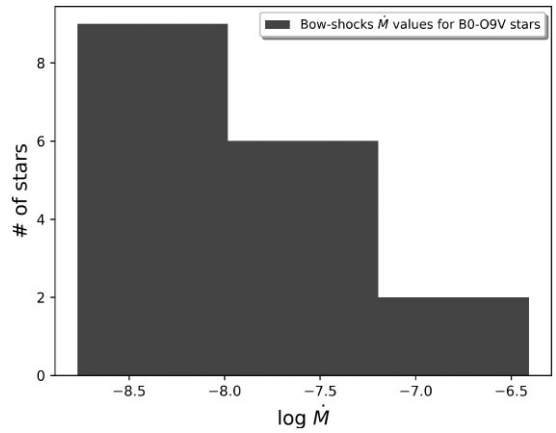

Figure 9. Histogram of mass-loss rates of B0-O9V stars from bow shocks measurements (Kobulnicky et al. 2019).

late O or early B dwarfs (O9-B0V), important in the context of the present study, they found mass-loss rate values ranging from $\sim 10^{-9}$ to $\sim 10^{-7}$ M$_\odot$ yr^{-1} (see their Fig. 11 and Table 3). This can be seen in Fig. 8, where the B0-O9V stars for example – emphasized as filled circles – span about 2 dex in wind strength, $\log D$.

To better illustrate this, we present in Fig. 9 the range of mass-loss rate values for the B0-O9V stars of Kobulnicky et al. work. A priori, a considerable range in mass-loss should be supported by very different UV spectral characteristics of these stars. However, the observations indicate otherwise, i.e. a fairly uniform UV morphology, with similar weak/very weak P-Cygni profiles at these spectral types (see e.g. Walborn, Nichols-Bohlin & Panek 1985). Therefore, we argue here that we should take the bow shocks results with some caution, at least when the scatter is high for specific spectral classes. Note that CMFGEN results for O9-O9.5V stars have $\dot{M} \sim 10^{-9}$ M$_\odot$ yr^{-1} (see Table 1).[7]

[7]One exception is HD 46202, where a single atmosphere model cannot fit the UV and optical data. This star has two measurements for the mass-loss rate. The UV based is in fact $\sim 10^{-9}$ M$_\odot$ yr^{-1}. The Hα based is $\sim 10^{-7}$ M$_\odot$ yr^{-1}, a discrepancy so far unsolved

The bow-shock method is not free from uncertainties. Through Monte Carlo calculations, the average uncertainty for the mass-loss rate estimated by these authors is about 40 per cent, neglecting dust emission coefficients and stellar peculiar velocities. In particular, dust emission coefficients can be changed in different ways (e.g. grain destruction by shocks), thus affecting $\dot{M}$, as discussed by Kobulnicky et al. (2019). Hopefully, future works will help estimate the magnitudes of these uncertainties.

In conclusion, bow-shocks measurement fall mostly below the predictions of Mokiem's relation and above the measurements made with CMFGEN. A reconciliation or at least the identification of the physical origin behind the discrepancy between both results (CMFGEN and bow-shocks) should be investigated in future studies.

5.4 Comparison with theoretical predictions

The main objective of this paper is the analysis of empirical data of the winds of O and B stars in the MW and SMC. Nevertheless, it is useful to compare our results also with theoretical predictions in the literature to check for trends and highlight possible problems. We will focus on the recent works by Björklund et al. (2021) and Vink & Sander (2021).

Björklund et al. (2021) predict mass-loss rates and terminal velocities for O-type stars in the MW and in the Magellanic Clouds, self-consistently. To solve the hydrodynamics, co-moving NLTE radiative transfer models are used to obtain the radiative force, in an iterative scheme. By comparing the three environments (SMC, LMC, and MW), the mass-loss rate dependence suggested was $\dot{M}(Z) \sim Z^{0.95}$ (i.e. $m = 0.95$), which is a mean. The value of m was observed to vary across the luminosity range, approximately as $m(L) = -0.32 \times (\log L/L_{\odot} - 6.0) + 0.79$. Roughly, it goes from about 1.2 at low L to 0.8 at high L, in contrast to our data tendency (see Fig. 4).

These authors compare their $\log \dot{M} \times \log L/L_{\odot}$ predictions for MW stars to others in the literature, namely from Vink et al. (2001), Lucy (2010), and Krtička & Kubát (2017). There is a considerable spread of $\dot{M}$ values for $\log L/L_{\odot} < 5.2$ (about ∼1 dex; see their fig. 5). That is, theoretical predictions do not agree at low L.

Regarding the observations, their theoretical WLR match well the observations of bright objects in the MW, that is, for $\log L/L_{\odot} > 5.2$. For the SMC, their $\log \dot{M} \times \log L/L_{\odot}$ predictions are in good agreement with the empirical values of Bouret et al. (2013), which we use in this paper.[8] By consequence, their WLR (SMC) is somewhat close to the one we obtain (see below).

In Fig. 10, we present the WLR obtained in this paper and from Björklund et al. (2021). We use their equation 19, for the MW and SMC metallicities. The physical units used in their work are modified to conform with ours. The expected proportionality between the wind strength and the luminosity, as well on metallicity, is apparent. However, a relatively stronger (weaker) Z dependence at low (high) L can be seen in the theoretical predictions – a fact that is emphasized by the authors – whereas our empirical data show otherwise (see also Fig. 4). At high L, their WLRs are below the ones inferred by us. The empirical data at low L naturally make the slopes of our fits higher. We provide an explanation for these differences behaviors below.

The predictions of Björklund et al. (2021) for MW low-L stars – $\log L/L_{\odot} < 5.0$ – are mass-loss rates from −8.28 to −8.04 ($\log \dot{M}$ units). The average is −8.14. This is higher than found from atmosphere models for O8-9.5V stars by up to an order of magnitude (see Table 1). For SMC stars, these authors predict at low-L mass-loss rates from −9.27 to −8.76 ($\log \dot{M}$ units). The average is −9.06. In contrast with the MW case, this is more in line with the rates obtained from atmosphere models (see Table 2).

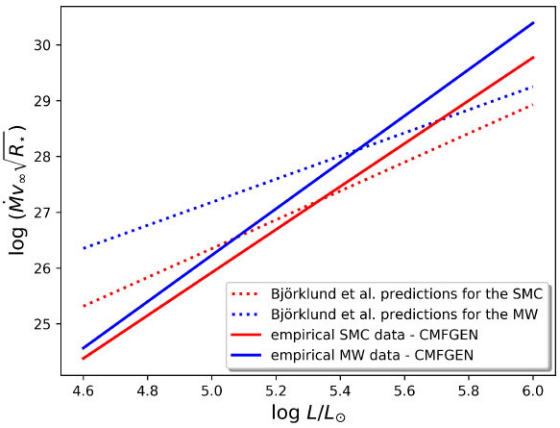

Figure 10. WLR comparison: theoretical calculations from Björklund et al. (2021) and our empirical (CMFGEN) data.

Therefore, at least part of the discrepancy with our results is related to the weak wind problem, which was discussed in Section 5. In short, hydrodynamics calculations indicate $\dot{M}$ values that are higher than inferred from observations, impacting the WLR – $D_{\rm mom} \propto \dot{M}$. For their MW models, the WLR slope is 2.07 ± 0.32. From our models, we get a much higher value, of 4.16 ± 0.23 (see Table 3). Regarding the SMC, our results indicate 3.85 ± 0.29 and Björklund et al. (2021) 2.56 ± 0.44, which is not a drastic difference as in the MW case.

In addition, we note that the terminal velocities of the low-L models of Björklund et al. (2021) are very high. For example, their $\log L/L_{\odot} = 4.91$ ($T_{\rm eff} = 33\,383$ K) model for an MW metallicity results in $V_{\infty} = 5411.75$ km s^{-1}. Values higher than about 3000 km s^{-1} are rarely reported from observations and deserve a deeper investigation (see e.g. Table 1 and Prinja et al. 1990). Such extreme velocities also help explain why their inferred relations are above ours – $D_{\rm mom} \propto V_{\infty}$. In fact, for MW stars with photospheric parameters close to the ones aforementioned, some observed V_{∞} values can be as low as ∼1000–2000 km s^{-1}. This represents a factor of ∼2.7–5.0 of difference, which translates to ∼0.4–0.7 dex in $\log D_{\rm mom}$.

Björklund et al. (2021) argued that such extreme velocities would not be seen in the UV wind diagnostics of low-L objects. That is, using UV P-Cygni profiles to obtain V_{∞} would be misleading as most of the wind is predicted to be shocked and at very high temperatures (Lagae et al. 2021). However, we note that some terminal velocities obtained from X-ray measurements are not very high. On the contrary, they seem to agree relatively well with the UV-based terminal velocities. For example, the late-type star ζ Oph has V_{∞}(UV) ∼ 1500 and V_{∞} (X-rays) ∼ 1400 km s^{-1} (Cohen et al. 2014). μ Col (O9.5V) is another example. Huenemoerder et al. (2012) report V_{∞}(X-rays) ∼ 1600 km s^{-1}, which agrees with the UV measurements within error bars[9] (Martins et al. 2005). Moreover, as discussed in Section 5, at a first glance, a very large (small) volume of hot gas seems incompatible

[8]Note that Björklund et al. (2021) mixed clumped and unclumped mass-loss rates data from table 2 of Bouret et al. (2013) in their comparison. Nevertheless, their fit is still reasonable when clumping corrections are taken into account, i.e. making clumped rates unclumped through $\dot{M}/\sqrt{f}$ = constant.

[9]Note that Huenemoerder et al. (2012) report that a good fit to O VIII (18.967, 18.973Å) can be also achieved with a terminal velocity of 2800 km s^{-1}, by increasing the value of the β parameter. Despite higher than the UV, this value is still much lower than reported by hydrodynamical predictions.

with the X-ray emission observed in these low-L (high L) massive stars.

Very fast winds are also reported in the predictions made by Vink & Sander (2021). Their dynamically consistent computations for the mass-loss rate and terminal velocity of massive stars update their previous work (Vink et al. 2001). For specific stellar masses and luminosity pairs, several Monte Carlo models were computed for different metallicities (from 1/33 to 3 $Z_{\odot}$) and temperatures.

Given the importance of the high terminal velocities found, Vink & Sander (2021) computed synthetic line profiles for specific models using the PoWR atmosphere code. In summary, they found strong absorption troughs in C IV λ 1549, exceeding 5000 km s^{-1}. However, it was shown that these troughs can be easily masked by carbon depletion at the surface, thanks to CNO mixing. Despite this effort, a deeper investigation is needed to address this issue. For example, stars close to the ZAMS are not expected to have strong carbon depletion and a priori could reveal such very fast wind signatures. A careful comparison with observed data is needed.

Regarding the metallicity dependence, for stars above the bi-stability jump – i.e. O stars range – Vink & Sander (2021) found that $\dot{M}(Z) \sim Z^{0.42}$, which is much weaker than inferred by Björklund et al. (2021). Their results also indicated that the modified momentum depends not only on L, but on $T_{\rm eff}$ as well, possibly hindering analyses as done here and in Mokiem et al. (2007).

The $T_{\rm eff}$ dependence of $D_{\rm mom}$ was observed by these authors exploring two temperature values, namely, 20 and 40 kK, over a luminosity interval from log $L/L_{\odot} \sim$ 5.0 to 6.0 (see their fig. 13). In brief, the wind momentum was found to be different for two stars with a same luminosity, if they possess different temperatures. Although the results are solid from a theoretical point of view, we note that there are no observed O stars with $T_{\rm eff}$ as low as 20 kK. They all possess temperatures above ∼28 kK (see e.g. Martins et al. 2005). Similarly, for example, there are no O stars with $T_{\rm eff} \sim 40$ kK at luminosities lower than log $L/L_{\odot} < 5.4$. Also, $T_{\rm eff}$s about 20 kK are reached by B supergiants, roughly at B1-2I spectral types, which are not present in our sample.

Hence, we do not have several stars in the parameters range where the $D_{\rm mom}$ dependence on $T_{\rm eff}$ was observed by Vink & Sander (2021). New calculations would be needed to address this issue. Alternatively, a careful comparison of a large sample of stars with specific spectral types would be desirable. For example, B1-2I and O5V stars have $T_{\rm eff}$ about 20 and 40 kK, respectively, and similar luminosities (log $L/L_{\odot} \sim$ 5.5). On average, their modified wind-momenta should be different by ∼0.5 dex, according to the theoretical results.

In conclusion, recent theoretical calculations obtain what is expected for line-driven winds, but still do not agree on the exact WLR and mass-loss rate dependence on metallicity. Our empirical WLRs are not matched, a fact that is probably linked to the weak wind problem and the very fast winds reported. Interestingly, these very fast winds seem to be a common feature of these recent theoretical solutions and should be carefully tested against multiwavelength observations.

5.4.1 *CAK-theory and the WLRs*

It is also interesting to compare our results, in particular the slopes of the WLRs obtained, with what is expected from the CAK equations. From first principles, the total radiative line acceleration is a sum of the contribution by optically thin and optically thick lines ($g_{\rm rad}^{\rm lines} = \sum_i g_i^{\rm thin} + \sum_i g_i^{\rm thick}$). The respective expressions are very different from one another, with the acceleration due to optically thick lines depending on the gradient of the velocity field.

In order to solve the hydrodynamics, these accelerations must be known at each wind depth point. This can be done by the use of a line-strength distribution function – in terms of an α power law – usually calculated from the opacities of thousands to millions of line transitions. The resulting expression is

$$g_{\rm rad}^{\rm lines} = \sum_i g_i^{\rm thin} + \sum_i g_i^{\rm thick} \propto N_{\rm eff} L \left(\frac{{\rm d}v/{\rm d}r}{\rho} \right)^{\alpha}, \quad (6)$$

where $N_{\rm eff}$ is the effective number of lines that drives the wind, ρ the gas density, and dv/dr the velocity gradient (see Kudritzki & Puls 2000; Puls, Springmann & Lennon 2000). With this acceleration (neglecting rotation), the hydrodynamics solution provides expressions for the velocity field and mass-loss rate, as a function of $\alpha' = \alpha + \delta$, where δ is the ionization parameter. The resulting mass-loss rate is $\dot{M} \propto N_{\rm eff}^{1/\alpha'} L^{1/\alpha'} (M(1-\Gamma))^{1-1/\alpha'}$, where Γ is the Eddington factor and $V_{\infty} \sim 2.25(\alpha/(1-\alpha))V_{\rm esc}$. The mass-loss depends not only on the number of effective lines but also on the luminosity and mass. However, the expression for the logarithm of the modified momentum ($\dot{M} V_{\infty} \sqrt{R/R_{\odot}}$), when α' is relatively close to 2/3, returns a weak or no mass dependence. Hence,

$$\log D_{\rm mom} \sim \frac{1}{\alpha'} \log L + {\rm const.} \quad (7)$$

Therefore, our inferred slopes – βs – can be directly compared with $1/\alpha'$. From Table 3, we can infer that[10]

$$\left(\frac{1}{\alpha'} \right)_{\rm SMC} < \left(\frac{1}{\alpha'} \right)_{\rm MW}, \quad (8)$$

that is, $\alpha_{\rm MW} < \alpha_{\rm SMC}$, neglecting δ (∼0.1). This leads to the conclusion that the radiative acceleration of the wind of SMC stars is higher than in the MW stars. By recalling the metallicities in these two environments, the contrary is expected. Thus, our results are in contradiction with the CAK-theory. However, this is not so surprising.

We note that the empirical data points at low luminosities have of course a huge influence on the derived slopes (see Fig. 2). These same points confront the radiatively driven wind theory, as we already discussed (weak wind problem; see Section 5). There is the possibility that these winds are not entirely CAK-driven, as been already pointed out in the literature (e.g. Muijres et al. 2012). Other physical mechanisms in addition to radiation pressure might be at play, invalidating the direct use of the equations above for simple estimates.

As a matter of fact, if we neglect the low-luminosity part of our WLR and focus on stars with log $L/L_{\odot} \gtrsim 5.4$, we find a lower slope for the MW ($\beta_{\rm MW} \sim 1.7$) and the SMC ($\beta_{\rm SMC} \sim 2.2$), satisfying $\alpha_{\rm MW} > \alpha_{\rm SMC}$ and thus what is expected in terms of line-statistics. Interestingly, in this case not only the slopes but the respective linear coefficients found (∼19.7 for the MW and ∼16.0 for the SMC) are in reasonable agreement with the ones found by Mokiem et al. (2007), within the error bars (see Table 3).

The low-L end of the WLR brings another difficulty. The detailed analysis on line-statistics presented by Puls et al. (2000) indicates that α decreases with $T_{\rm eff}$, in thin winds and/or low-Z environments. These conditions are met exactly at low L in our sample. Indeed, our empirical slopes imply $\alpha \sim 1/4$. This was also previously reported

[10]Do not confuse the αs used in this section with the linear coefficients listed in Table 3.

by Martins et al. (2005), from their sample of O dwarfs. From a theoretical point of view however, when α values are very distinct from 2/3, equation (7) can present an important mass term, which is neglected.

Overall, it can be said that our WLRs follow well the CAK theory equations for objects with dense winds, i.e. the brighter objects. However, difficulties and contradictions arise when low-L objects are considered.

6 CONCLUSIONS

We gathered empirical data of several MW and Small Magellanic O and B stars of several spectral classes. Most of them were analysed by our group along the years, using the CMFGEN code. We analysed the data to address the empirical metallicity dependence of wind properties. The main results of our paper are summarized below:

(i) Based on CMFGEN models that consistently fit the UV and optical spectra of massive OB stars, we found a clear dependence of the wind strengths on luminosity and metallicity, as expected by the radiatively driven wind theory.

(ii) We improved the analysis presented by Mokiem et al. (2007), regarding MW x SMC stars. We analysed a large luminosity range, in contrast with their work, and explored the luminosity dependence of the Z dependence of the mass-loss rate. We used our results to estimate and visualize the m values of the $\dot{M} \sim Z^m$ relation, which is widely used in the literature. We found m values of $\sim$0.5−0.8, when $\log L/L_\odot$ is $\gtrsim$5.4 (i.e. bright objects). However, the Z dependence seems to get weaker at low L. If confirmed by more data, this last finding has likely important astrophysical consequences (e.g. angular momentum evolution, mixing).

(iii) We also analysed wind strengths giving weight to Hα mass-loss rate measurements. The Z dependence remains, but it does not get weaker at low L. We discussed that Hα is not free from uncertainties (e.g. contamination, line filling) and there is no reason to favour Hα over UV measurements. It is more reliable to consider results that are based on consistent fits to these two spectral regions.

(iv) The terminal velocities of the stars of our sample also suggest a Z dependence. SMC stars seem to have lower terminal wind speeds than MW stars, on average. We estimated the n exponent in the $V_\infty \sim Z^n$ relation to be $\sim$0.1–0.2, further supporting the widely used relation provided long ago by Leitherer et al. (1992). However, a larger sample should be analysed to confirm our results, as discussed in Section 4.

(v) Our derived wind strengths for SMC stars are in good agreement with the ones inferred recently by Ramachandran et al. (2019), based on an independent radiative transfer code (PoWR). This brings support to the WLR obtained with CMFGEN and the inferred Z dependence.

(vi) Mass-loss rate and $\log D$ measurements based on bow shocks around O and B stars in the MW (Kobulnicky et al. 2019) present a large scatter at low luminosities. In the WLR, they fall mostly above the CMFGEN results. The large range in $\dot{M}$ values for B0-O9V stars obtained by this method should be further investigated, since they are likely in contrast to the fairly uniform UV wind features of these objects.

(vii) Theoretical calculations carried out by different authors find the metallicity dependence of the mass-loss rates of massive stars, but the values reported are not precise. The m exponents (in $\dot{M}(Z) \sim Z^m$) vary considerably, but are close to our results. Part of the discrepancy between our results and theory at low L is likely linked to the weak wind problem and the very high terminal velocities predicted (e.g. greatly exceeding 3000 km s^{-1}). Despite the complexities and known limitations of NLTE expanding atmosphere models, the data provided here have an empirical nature and should serve as a guide for future comparisons.

(viii) We compared the slopes of our WLRs to what is expected in terms of the CAK equations. Regarding line-statistics, contradictory results are obtained due the low-luminosity stars of our sample – $\alpha_{\rm SMC} > \alpha_{\rm MW}$. When this region is neglected, no contradictions arise and our WLRs are in good agreement with the ones previously obtained by Mokiem et al. (2007). We attribute the issue at low L to the weak wind problem and also a possible misuse of the CAK equations. Other physical mechanisms in addition to radiation pressure might be at play, invalidating the direct use of CAK equations for simple estimates.

It would be helpful to increase the sample of analysed stars using optical and UV data, consistently. In this context, the Hubble UV Legacy Library of Young Stars as Essential Standards (ULLYSES) will be an excellent opportunity in the next years. Robust mass-loss rates for Magellanic Clouds stars would provide better constrains on the relations provided in this work.

ACKNOWLEDGEMENTS

WLFM acknowledges CNPq for the PQ grant (307152/2016-2) and John Hillier for making CMFGEN available to the massive star community. MBP gratefully acknowledges funding from the German Deutsche Forschungsgemeinschaft, DFG, in the form of an Emmy Noether Research Group (grant number SA4064/1-1, PI: Sander).

DATA AVAILABILITY

The data underlying this paper are available in this paper.

REFERENCES

Abbott B. P. et al., 2016, ApJ, 818, L22
Abbott D. C., 1982, ApJ, 263, 723
Björklund R., Sundqvist J. O., Puls J., Najarro F., 2021, A&A, 648, 36
Bouret J.-C., Lanz T., Hiller D. J., 2005, A&A, 438, 301
Bouret J.-C., Hiller D. J., Lanz T., Fullerton A. W., 2012, A&A, 544, 67
Bouret J.-C., Lanz T., Martins F., Marcolino W. L. F., Hillier D. J., Depagne E., Hubeny I., 2013, A&A, 555, 1
Bouret J.-C., Lanz T., Hillier D. J., Martins F., Marcolino W. L. F., Depagne E., 2015, MNRAS, 449, 1545
Bouret J.-C., Martins F., Hillier D. J., Marcolino W. L. F., Rocha-Pinto H. J., Georgy C., Lanz T., Hubeny I., 2021, A&A, 647, 134
Brott I. et al., 2011, A&A, 530, 115
Castor J. I., Abbott D. C., Klein R. I., 1975, ApJ, 195, 157
Cohen D., Wollman E. E., Leutenegger M. A., Sundqvist J. O., Fullerton A. W., Zsargó J., Owocki S. P., 2014, MNRAS, 439, 908
Crowther P. A., Lennon D. J., Walborn N. R., 2006, A&A, 446, 279
de Almeida E. S. G., Marcolino W. L. F., Bouret J.-C., Pereira C. B., 2019, A&A, 628, 36
Doyle T. F., Petit V., Cohen D., Leutenegger M., 2017, in Eldridge J. J.et al. eds, Proc. IAU Symp. 329, The Lives and Death-Throes of Massive Stars. Kluwer, Dordrecht, p. 395
Ekström S. et al., 2012, A&A, 537, 146
Flores B. L., Hillier D. J., 2021, MNRAS, 504, 311
Fullerton A. W., Massa D. L., Prinja R. K., 2006, ApJ, 637, 1025
Garcia M., Herrero A., Najarro F., Lennon D. J., Urbaneja M. A., 2014, ApJ, 788, 64
Georgy C. et al., 2013, A&A, 558, 103
Gvaramadze V. V., Langer N., Mackey J., 2012, MNRAS, 427, 50
Harries T. J., Hilditch R. W., Howarth I. D., 2003, MNRAS, 339, 157

Henney W. J., Arthur S. J., 2019, MNRAS, 489, 2142
Hillier D. J., Miller D. L., 1998, ApJ, 496, 407
Huenemoerder D. P., Oskinova L. M., Ignace R., Waldron W. L., Todt H., Hamaguchi K., Kitamoto S., 2012, ApJ, 756, L34
Kobulnicky H. A., Chick W. T., Povich M. S., 2019, AJ, 158, 73
Krtička J., Kubát J., 2017, A&A, 606, 31
Krtička J., Kubát J., 2018, A&A, 612, 20
Kudritzki R.-P., Puls J., 2000, ARA&A, 38, 613
Lagae C., Driessen F. A., Hennicker L., Kee N. D., Sundqvist J. O., 2021, A&A, 648, 94
Lamers H. J. G. L. M., Cassinelli J. P., 1999, Introduction to Stellar Winds. Cambridge Univ. Press, Cambridge
Leitherer C., Robert C., Drissen L., 1992, ApJ, 401, 596
Lépine S., Moffat A. F. J., 2008, AJ, 136, 548
Lucy L. B., 2010, A&A, 512, 33
Mahy L., Rauw G., De Becker M., Eenens P., Flores C. A., 2015, A&A, 577, 23
Maíz-Apellaníz J. et al., 2016, ApJS, 224, 4
Marchenko S. V., Foellmi C., Moffat A. F. J., Martins F., Bouret J.-C., Depagne E., 2007, ApJ, 656, 77
Marcolino W. L. F., Bouret J.-C., Martins F., Hillier D. J., Lanz T., Escolano C., 2009, A&A, 837, 852
Marcolino W. L. F., Bouret J.-C., Lanz T., Maia D. S., Audard M., 2017, MNRAS, 470, 2710
Martins F., 2011, Société Royale des Sciences de Liège, Bulletin, 80, 29
Martins F., Schaerer D., Hillier D. J., Meynadier F., Heydari-Malayeri M., Walborn N. R., 2005, A&A, 441, 735
Martins F., Mahy L., Hillier D. J., Rauw G., 2012, A&A, 538, 39
Martins F., Marcolino W., Hillier D. J., Donati J.-F., Bouret J.-C., 2015, A&A, 574, 142
Meynet G., Maeder A., 2000, A&A, 361, 101
Mokiem M. R. et al., 2007, A&A, 473, 603
Muijres L. E., Vink J. S., de Koter A., Muller P. E., Langer N., 2012, A&A, 537, 37
Oskinova L. M., Feldmeier A., Hamann W.-R., 2006, MNRAS, 372, 313
Owocki S. P., Castor J. I., Rybicki G. B., 1988, ApJ, 335, 914
Prinja R. K., Barlow M. J., Howarth I. D., 1990, ApJ, 361, 607
Prinja R. K., Massa D., Searle S. C., 2005, A&A, 430, L41
Puls J., Springmann U., Lennon M., 2000, A&A, 141, 23
Puls J., Vink J. S., Najarro F., 2008, ARA&A, 16, 209
Ramachandran V. et al., 2019, A&A, 625, 104
Ramírez-Agudelo O. H. et al., 2017, A&A, 600, 81
Sabín-Sanjulián C. et al., 2017, A&A, 601, 79
Sana H., Rauw G., Nazé Y., Gosset E., Vreux J.-M., 2006, MNRAS, 372, 661
Searle S. C., Prinja R. K., Massa D., Ryans R., 2008, A&A, 481, 777
Sundqvist J. O., 2013, Massive Stars: From Alpha to Omega. Rhodes, p. 47
Sundqvist J. O., Puls J., 2018, A&A, 619, 59
Sundqvist J. O., Björklund R., Puls J., Najarro F., 2019, A&A, 632, 126
Therneau T., 2018, deming: Deming, Theil-Sen, Passing-Bablock and Total Least Squares Regression. R package version 1.4
Vilhu O., Kallman T. R., 2019, preprint (arXiv:1906.05581)
Vink J. S., Sander A., 2021, MNRAS, 504, 2051
Vink J. S., de Koter A., Lamers H. J. G. L. M., 2001, A&A, 369, 574
Walborn N. R. et al., 2002, AJ, 123, 2754
Walborn N. R., Nichols-Bohlin J., Panek R. J., 1985, NASA Ref. Publication, NASA-RP-1155
Whalen D. J. et al., 2014, ApJ, 797, 9

This paper has been typeset from a TEX/LATEX file prepared by the author.